Lorenzo B. Kunkels

Influence of interspace and controlled disorder on bactericidal properties of nanopatterns

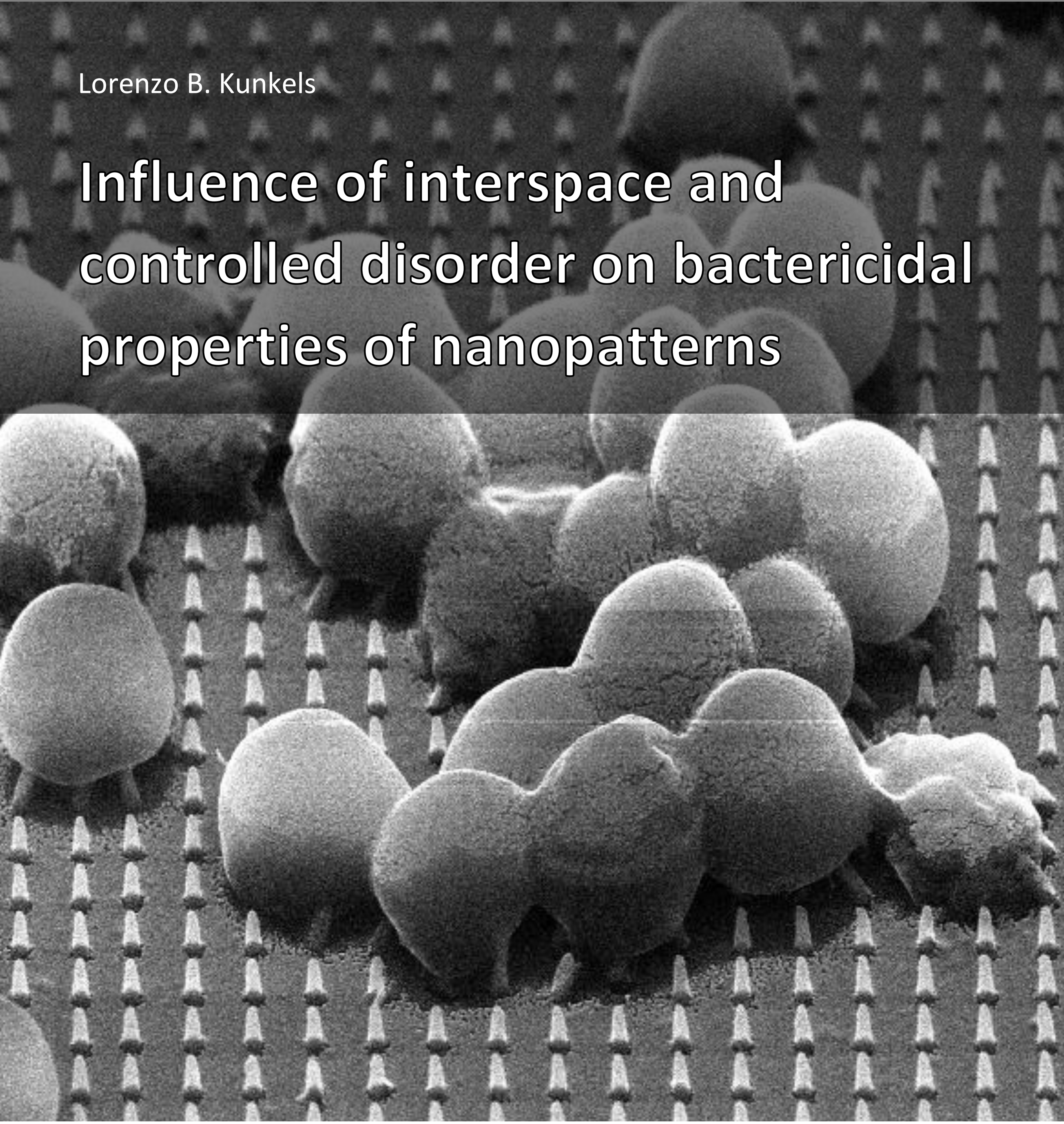

Influence of interspace and controlled disorder on bactericidal properties of nanopatterns

By

Lorenzo B. Kunkels

4301536

in partial fulfilment of the requirements for the degree of

Master of Science

in Biomedical Engineering

at the Delft University of Technology,

to be defended publicly on September 19, 2019.

Supervisor:	Dr. ir. Amir A. Zadpoor	TU Delft
	Dr. ir. Lidy E. Fratila-Apachitei	TU Delft
	Dr. ir. Cornelis W. Hagen	TU Delft
	Dr. ir. Peter-Leon Hagedoorn	TU Delft

This thesis is confidential and cannot be made public until 13-9-2021.

September 13, 2019

TU Delft

Abstract

Patients with orthopaedic implants often experience implant-associated infections (IAI), one of the most prominent causes for implant failure. IAIs are caused by pathogens adhering to the implant surface. One method to prevent IAIs is through the use of surface topography modifications. Cellular behaviour has been shown to be influenced by substrate surface topographies. Ideally, a topography that can simultaneously kill bacteria and promote osseointegration is desirable. In previous research, proved-to-be-bactericidal nanopillars of ~180 nm in height and ~80 nm in diameter were fabricated at 170 nm interspace, resulting in a bactericidal efficiency of 36 ± 5% for *Staphylococcus aureus (S. aureus).* The current research aimed to enhance this bactericidal efficiency by producing nanopatterns with different interspace distances and introducing disorder, while keeping the same nanopillar dimensions. The patterns have been produced by using electron beam induced deposition (EBID) at 100, 170, 300 and 500 nm interspacing. A disordered version of the 170, 300 and 500 nm samples was included with 45, 110 and 210 nm disorder distance, respectively. In order to keep the nanopillar dimensions consistent, EBID parameters were systematically optimised. The nanopatterns were interfaced with *S. aureus* cells and the bactericidal efficiencies were determined by counting the number of healthy, deformed and dead bacterial cells. For the ordered 100, 170, 300 and 500 nm interspace nanopatterns, bactericidal efficiencies of 62.3 ± 23.1%, 45.0 ± 31.4%, 8.6 ± 4.2% and 3.7 ± 2.3% were found, respectively. For the disordered 170, 300 and 500 nm interspace nanopatterns, bactericidal efficiencies of 45.9 ± 29.2%, 14.7 ± 7.2% and 12.7 ± 9.8% were found, respectively. These results showed a significantly higher bactericidal effect on lower-interspace nanopatterns. Disordered nanopatterns showed only slightly higher bactericidal efficiencies when compared to the ordered nanopatterns. This data indicated that bactericidal efficiencies could be increased relative to the previous nanopattern design. The findings of this research aid in developing antibacterial nanopatterns that are capable of killing gram-positive bacteria and support the path to prevention of IAIs.

KEY WORDS. Bactericidal • nanopatterns • nanoscale additive manufacturing • electron beam induced deposition • antibacterial • nanopillars • topography modification • nanostructured surfaces

Table of Contents

1. Introduction

Patients with orthopaedic implants often experience implant-associated infections (IAI), one of the most prominent causes for implant failure [1]. IAIs are caused by pathogens, which include different bacterial types, adhering to the implant surface. These pathogens grow and eventually form biofilms, which the immune system of the host cannot easily counter by itself [2]. Because of this, implant functions get inhibited and the infections result in significant morbidity or even mortality [3]. These pathogens are often resistant to the defence system of the host and most antibiotics, meaning surgery is often the last option of treating the problem. This can be a significant risk to the patient, as the IAIs are not only caused by post-operative proliferation of bacteria in the wound, but also by the introduction of microorganisms through inadequately sterilized surgical instruments and implants [4]. For example, the Medicare Inpatient Data Set (United States) from 2005 to 2015 was analysed. This data showed survival for more than 5 years for only 67% for periprosthetic joint infection (PJI) after total hip arthroplasty and 72% for IAIs after total knee arthroplasty [5]. In addition to causing problems for the patients, an increase of 300% or higher in healthcare costs is expected [6].

Instead of focussing on the treatment of IAIs it is thus of greater importance to focus on their prevention. One of the methods by which this can be achieved is through antibacterial surfaces [7]. Using these surfaces, prevention of bacterial adhesion and/or killing of adhered bacteria on the implant surface is made possible. Many of these surfaces, however, prevent all types of cells from adhering to the implants. As this means osseointegration is inhibited, such a solution is not viable for countering IAIs, as osseointegration is crucial for implant integration in the body. Thus, it is of importance to utilise implant surfaces that kill bacteria and promote host cell proliferation simultaneously [8]. One method of achieving such implant properties is the use of chemical treatments. Chemicals include antibiotics [9, 10], bactericidal nanoparticles such as silver [11-13], or other antibacterial agents such as triclosan or lysozyme [14]. However, when using chemicals, a chance of bacterial resistance build-up on the long-term exists, which suggests another method would be necessary in the future [15-17]. Therefore, it may be more viable to use an alternative option: surface topography modifications. Cellular behaviour has been shown to be influenced by substrate surface topographies. These topographies are capable of affecting cellular functions such as proliferation, differentiation and matrix formation, as well as cell selection and cell alignment [18]. The size of these surface features have been proven to be of importance, as macroscale (>100 µm) features affect cells colonies, microscale (0.1 – 100 µm) features affect single cells, and nanoscale (1 – 100 nm) features may affect individual cell receptors [19]. The submicron- and nanoscale surface features have proven capable of killing bacteria through mechanical pathways [20, 21] of which examples have additionally been found in nature [22, 23]. Aside from the size of the topography features, another factor that influences cell behaviour is their spatial arrangement [24, 25]. The exact effect of topographical feature spatial arrangement is a topic of ongoing research, for which recent improvements in micro- and nanoscale fabrication techniques offer researchers access to methods of artificially creating such patterns. These patterns can be highly customized to suit the variable of research. For instance height, diameter and interspace can be designed as preferred to create custom patterns, often taking inspiration from pattern characteristics found in nature [26, 27]. To be able to accurately and reproducibly fabricate these patterns, a technique should be used that allows for the fabrication of structures with nanoscale features [28].

One method that suits this is *electron beam induced deposition* (EBID), a nanoscale additive manufacturing method that allows for the production of features with sizes of down to several nanometres [29-32]. EBID directly forms nanoscale structures using the electron beam from a scanning electron microscope (SEM) in the presence of a gas precursor. For this process, focused probe optics (beam acceleration voltage, probe current, probe size, imaging performance), the substrate (material, temperature, conductivity, cleanliness) and gas delivery (precursor type, precursor temperature, pressure, molecular flux at the substrate surface) each influence the morphology of the deposited structures (see Appendix A5). Additionally, parameters that control the total exposure time of a structure (for example dwell time) directly affect the shape of the structure and should be optimized to get the exact result that is preferred.

Staphylococcus aureus (*S. aureus*, gram-positive) and *Escherichia coli* (*E. coli*, gram-negative) bacteria are two types of bacteria isolated from 33-43% and 4-7% cases of IAIs respectively [33]. Such higher virulence organisms are dominant in early-onset infections [34]. In previous research using EBID, it was demonstrated that nanopillars with a height of 180 nm, a diameter of 80 nm and interspacing of 170 nm are bactericidal against these two types of bacteria. At these nanopillar dimensions, bactericidal efficiencies of 36 ± 5% and 97 ± 1% were achieved for *S. aureus* and *E. coli*, respectively. Simultaneously, these pillars are likely to promote osteogenic growth, as found in literature describing bactericidal and/or osteogenic activities of nanopatterns [35] (Figure 1). Although this data is promising, there is still a need to enhance the bactericidal efficiency for *S. aureus*. In addition, there is a lack of knowledge with regards to the exact effect of interpillar spacing on the bactericidal efficiency of nanopatterns. Besides interspace, it is not known what influence a disordered distribution (in contrast to a true-square arrangement) of these pillars has on the bactericidal capacities. In nature, antibacterial nanopatterned surfaces have been found (e.g., cicada wings, dragonfly wings, gecko skin) that demonstrate a variety of bactericidal potencies. These natural nanopatterns exist with different interspaces and grades of disorder, also shown in Figure 2 [22, 36-41]. However, these patterns have multiple varying parameters (pillar height, diameter, spacing, disorder), which means no clear information on the effect of each single parameter is available. To fill this lack of knowledge, this study focuses on the influence of interspace and controlled disorder on the bactericidal properties of nanopatterns while keeping the nanopillar height and diameter constant. The bacteria used for the assessment of bactericidal efficiency were limited to *S. aureus*, as a satisfactory high killing efficiency was already found for *E. coli*. In addition, this allows for a clear focus on one of the most predominant bacteria in IAIs. The nanopatterns were produced using EBID with four different interspace distances of 100, 170, 300 and 500 nm. For the 170, 300 and 500 nm interspace patterns disordered versions were also produced, with 45, 110 and 210 nm displacement from a true-square arrangement respectively. This amounts to seven distinctive nanopatterns.

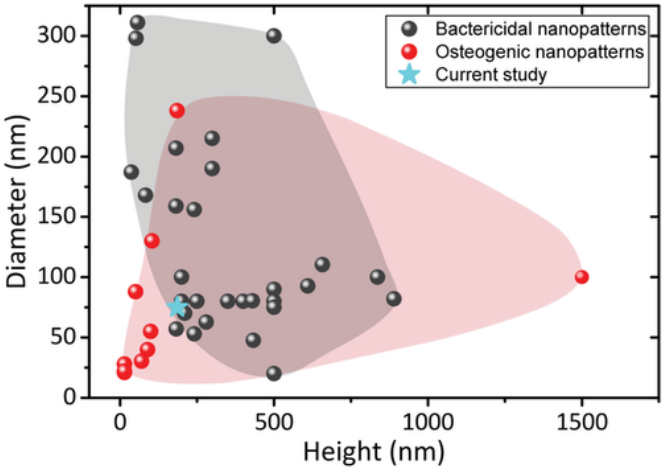

Figure 1. Comparing nanopillar dimensions (height and diameter) with respect to their bactericidal and osteogenic potency, based on data found in literature. The graph illustrates that nanopillars with heights of ~180 nm and diameters of ~80 nm are likely to possess both osteogenic and bactericidal properties [35].

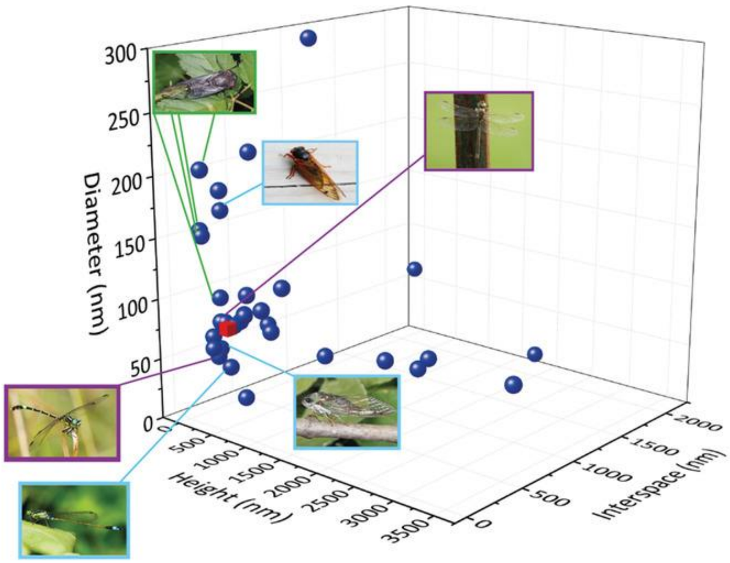

Figure 2. Bactericidal nanopatterns found in literature. The red square represents the 170 nm interspacing pattern used in previous research [35]. The interspaces used in this study are inspired by the naturally occurring bactericidal nanopatterns shown in this graph [35].

This report first details the methods used for fabrication of the nanopatterns, followed by the methods used to culture the *S. aureus* bacteria and to inoculate the produced nanopatterns. Next, the results section characterizes the fabricated nanopatterns with regards to their dimensions. After this, the results of the bacterial cultures are presented and bactericidal efficiencies of the different nanopatterns are compared. Finally, in the discussion, these results are related to literature, where possible explanations about the significant differences between the nanopatterns are given.

2. Materials and Methods

2.1 Nanopattern fabrication and characterization

2.1.1 Equipment

As the substrate for nanopattern deposition, silicon wafers were used. These double-sided polished silicon wafers (thickness 525 ± 25 µm, p-type <100>, 0-100 Ohm*cm) were cut into 1 × 1 cm^2 samples. These wafers, after soaking in nitric acid for 15 minutes, were rinsed twice with deionized water, then dried with compressed nitrogen gas and heated at 90°C on a hotplate to minimize the contamination of the sample surface. After the samples dried, they were spin-coated with AZ5214 photoresists at 4000 rpm and then baked on a hotplate at 110°C for one minute. The resist on the edges of the sample was removed using an acetone-coated cotton swab. Etching was performed on the corners of the samples by inductive coupled plasma reactive ion etching (ICP RIE) (Adixen, AMS100 Bosch, l-speeder) for ~5 seconds to form black silicon [42] to aid in the initialization steps of the electron microscopy. Finally, the samples were rinsed in acetone and spin-dried [35].

EBID was used to pattern three areas with a dimension of 20 × 20 μm^2 with the Nova Nano Lab 650 Dual Beam (FEI company, OR, USA) and Helios Nano Lab 650 (FEI company, OR, USA). These systems contain an electron beam, used for material deposition. With these systems, both deposition and SEM imaging of the nanostructures can be done in situ. To be able to work at ultrahigh resolutions (down to several nanometres [32]), the EBID process was performed in immersion mode. The electron beam voltage and current were set to 17.8 kV and 0.60 nA respectively for the Nova, working in an electron-limited regime. As the Helios did not allow a current of 0.60 nA, its current was instead set to 0.40 nA. However, due to the additional differences in current measurement accuracy and precursor gas preheating temperature (39°C for the Nova and 44°C for the Helios), this resulted in roughly the same pillar dimensions as the Nova would have produced. To prevent sample-contamination during deposition, the microscope was rested after insertion of the substrate until a chamber pressure lower than 4.00 e^{-6} mbar was reached. For the Nova and Helios, the working distances were ~5 mm and ~4 mm respectively. The nanopatterns were formed using the precursor gas trimethyl(methylcyclopentadienyl)-platinum(IV), $(CH_3C_5H_4)Pt(CH_3)_3$, $MeCpPtIVMe_3$, or $C_9H_{18}Pt$, heated to 39°C for the Nova and 44°C for the Helios. The gas was injected using a gas injection system (GIS) needle at a distance of ~140 µm above the sample [35].

2.1.2 Electron-beam induced deposition (EBID)

The EBID process directly deposits nanoscale structures on a substrate using the electron beam from a scanning electron microscope (SEM). Precursor gas molecules are introduced into the vacuum chamber in close proximity to the substrate. These precursor molecules are adsorbed onto the substrate surface after which the electron beam is activated. The electrons dissociate the precursor molecules, resulting in volatile- and non-volatile fragments. The volatile fragments are pumped out of the chamber, while the non-volatile fragments adhere to the substrate, forming the solid structures that together define the surface topography. By repeatedly exposing the same structures to this process they grow in width and height. This means that the total exposure time of a certain location on the substrate is directly related to the morphology of the formed structure. As of such, the structure dimensions can be accurately defined within the range of a few nanometres. A schematic of the EBID procedure is shown in Figure 3.

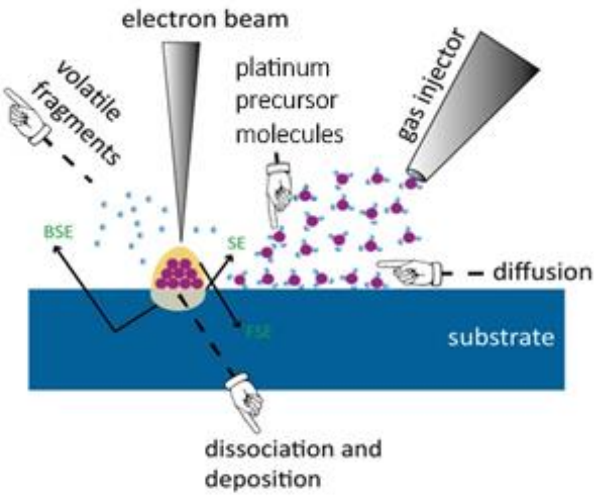

Figure 3. Electron beam focused upon a surface. Transiently adsorbed precursor molecules provided by a gas injection system (GIS) are dissociated by the electron beam, creating volatile- and non-volatile fragments. Volatile fragments are pumped out of the system, while non-volatile fragments form solid structures. Primary electrons (PE) hit the substrate or deposited structure, forming secondary electrons (SE), backscattered electrons (BSE) and forward scattered electrons (FSE) [29, 35].

2.1.3 Nanopattern fabrication

Single-dot exposure was used as the writing strategy, using stream files (see Appendix A6) generated through MATLAB (MathWorks, US) scripts (Appendix A9). These stream files determine the positions of the pillars used to form a given area of the nanopatterns, in addition to the dwell time, number of repeats, number of passes and refresh time. The definitions of these parameters are as follows:

- **Dwell time**: the time each position (centre of pillar) is exposed to the electron-beam. The dwell time is applied for each repeat and each pass.
- **Refresh time**: it is possible for precursor gas to be injected at a lower rate than required for deposition in the electron-limited regime, resulting in a depletion of precursor gas on the substrate, essentially forming a precursor-limited regime. To prevent or limit this, refresh time introduces a delay before and after each exposure.

- **Repeat**: number of times a position is exposed before moving on to the next position.
- **Pass**: number of times the whole stream file is written, meaning that for multiple passes the beam moves back to the first position after the final position has been exposed.

Together, these parameters influence the following values:

- **Exposure time per pillar**: the time one pillar is exposed to the electron-beam, thus
$$t_{exposure} = dwell\,time * repeats * passes$$
- **Time to pattern array**: The total time needed to pattern a given area. This includes all pillars in the array and the above mentioned parameters. This parameter is calculated solely for user reference.

To produce nanopatterns with the required dimensions, the stream file parameters were selected based on previous research [35]. To account for any stage drift that could be present with use of the electron microscopes, which causes deposition to occur away from the pillar centre over time and thus resulting in varying pillar dimensions, it was chosen to use a single pass with a variable amount of repeats. The disadvantage, however, is the fact that the precursor at the repeatedly exposed location may deplete faster than it is introduced. This may result in the system no longer operating in the electron-limited regime and thus causing slower structural growth. To counter this effect, the refresh time has been increased to 20 µs based on observations of the effect intensity, performed during the internship [43]. However, the refresh time does not completely remove the difference in dimensions. Even with refresh times in the order of seconds there will still be a difference between pillars in opposing corners, caused by the proximity effect (which is intensified when using repeats instead of passes due to the electrons colliding with fully deposited pillars, see Appendix A5). In addition to the other pattern variables used, an extra variable was introduced with respect to the previously performed research, namely the disorder distance. This variable determines the maximum pillar-displacement from the true-square arrangement. The disorder distance was set to the maximum distance at which pillars do not intersect (Appendix A7).

The interpillar spacings used in this study were based on found literature and the naturally occurring bactericidal nanopatterns mentioned before (while keeping the pillar height and diameter constant, in contrast to the available literature). Starting from an interspace of 170 nm, as in previous research [35], it was chosen to design the other patterns with interspace distances larger and smaller than 170 nm. Due to the potential difference in experimental circumstances, the 170 nm pattern was also produced as a control sample. As the diameter of 80 nm inhibits the use of interspacing below 80 nm (which would merge pillars together due to their dimensions) and still using a significantly different value from 170 nm, the pattern with a smaller interspace was given a spacing of 100 nm. This value was also based on found evidence of nanopatterns with similar spacings exhibiting a bactericidal efficiency of 73% on *S. aureus* [44]. That study, however, used a nanopattern consisting of 432.5 ± 63.5 nm high pillars, where the height might possibly influence the bactericidal effect of nanopatterns. For the patterns with larger spacing, it was chosen not to exceed 500 nm interspace. This is due to *S. aureus* bacteria having diameters of ~600 nm [45] and would thus be able to navigate in between pillars with larger interspaces. To also include a pattern with an intermediate value of interspace, a 300 nm interspace pattern was chosen to be produced based on studies showing potential bactericidal efficiencies of 31% on *S. aureus* [46]. The study that achieved this efficiency used nanopillars of ~150 nm. To test the effect of pillar arrangement disorder on the antibacterial potency of the patterns, each pattern is to be produced once without disorder and once with maximum disorder. Table 1 shows an overview of the different pattern designs.

Table 1*: Overview of the different nanopattern designs together with their denoted pattern name. Interspacing and maximum disorder distance differs per pattern.*

Pattern name	Interspace (Δ) [nm]	Disorder distance (Ψ) [nm]
100s0d	100	0
170s0d	170	0
170s45d	170	45
300s0d	300	0
300s110d	300	110
500s0d	500	0
500s210d	500	210

The settings used in the stream files for the designed nanopatterns are displayed in Table 2. Due to the Nova and Helios having different system variables (such as working distance and precursor temperature), the parameters differ depending on the used system and system conditions. Using these settings, the nanopatterns were produced to have a pillar shape (similar to droplet-shaped structures).

Table 2*: Electron beam and stream file settings per nanopattern design. The 100 nm interspace pattern has not been produced using the Nova.*

Electron microscope	Interspace (Δ) [nm]	Disorder distance (Ψ) [nm]	Array size [rows × columns]	Dwell time [ms]	Blur [nm]	Repeats [-]	Passes [-]	Refresh time [µs]	Array time [min:s]
Nova	170	0, 45	40x40	3	0	100	1	20	08:03
	300	0, 110	23x23	8	26	100	1	20	07:04
	500	0, 210	14x14	8	26	100	1	20	02:37
Helios	100	0	67x67	5	0	50	1	20	18:46
	170	0, 45	40x40	3	0	100	1	20	08:03
	300	0, 110	23x23	3	20	100	1	20	02:40
	500	0, 210	14x14	3	20	100	1	20	00:59

Each of the seven nanopatterns was fabricated in triplicate (three areas of 20 × 20 μm^2) per sample using the conditions named before, as illustrated in Figure 4. The experiments were performed in duplicate, meaning each pattern type was tested twice, forming a total of 14 produced samples or 42 patterned areas (20 × 20 μm^2).

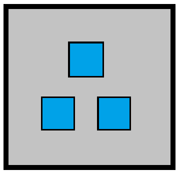

Figure 4. Schematic of a nanopatterned sample (proportions not to scale). Three patterned areas (20 × 20 µm^2) with the same interspace and disorder values were produced on a 1 × 1 cm^2 silicon wafer.

2.1.4 Nanopattern characterization by SEM and AFM

To analyse the characteristics of the deposited nanopatterns, SEM imaging was performed at a brightness setting of around ~40.6% and a contrast setting of around ~68.0% for the Nova. A brightness of ~36.9% and contrast ~50.8% were used for the Helios. A resolution of 1024 × 884 pixels was used. As pillar dimensions might differ depending on the location in the array (as stated before), images were made in the middle of the array. The images were made at multiple magnifications and the stage was tilted 0° and 52° with respect to the electron beam to obtain both top-down and diagonal images of the nanopatterns. Using the Nova or Helios software, or the Gwyddion software (version 2.52), pillar dimensions were measured using cross-section tilt correction, where pillar height is defined from the top of the pillar to the centre of its base (measured at 52° stage tilt) and pillar diameter is the width of its base. No changes to electron beam voltage or current were made with respect to those used during deposition. At the end of patterning, images were made of the total pattern area for the sake of providing a clear overview. To further characterize the nanopatterns they were also imaged using atomic force microscopy (AFM) with a Dimension FastScan AFM (Bruker, Billerica, USA) in the ScanAsyst mode. A scan rate of 0.5 Hz and a TESPA-HAR probe having a nominal spring constant of 42 N m^{-1} and a nominal tip radius of 10 nm were used.

2.1.5 Nanopattern wettability

In addition, calculations were performed to determine the water contact angle of the nanopatterns in order to assess wettability. These calculations were based in previous research [35], where a thin Pt-C layer was deposited on a silicon wafer to identify the static contact angle of Pt-C material (θ_0) by a drop shape analyser (DSA 100, Kruss, Hamburg, Germany) using deionized water. 2 µL liquid with a falling rate of 1667 µL min^{-1} was placed on the surface using a syringe. After 5 s of the droplet resting on the surface, the contact angle figure was recorded. The measurement reported the average contact angle within 30 s after the whole droplet volume touching the substrate. As the nanopatterns were too small compared to the droplet, their contact angles were calculated using the Cassie-Baxter wettability model. To do so, it was assumed air was trapped between the nanopillars [35]. The Cassie-Baxter contact angle (θ_c) is given by

$$\cos(\theta_c) = \varphi(\cos(\theta_0) + 1) - 1$$

where φ and θ_0 are the solid fraction (ratio between the nanopillar tip area and the projected surface area) and the contact angle of the flat Pt-C surface, respectively. The solid fraction was calculated by

$$\varphi = \frac{\pi d^2}{4i^2}$$

where *d* represents the nanopillar tip diameter and *i* is the nanopillar interspacing. In order to calculate the solid fraction, the tip diameters of several nanopillars (N = 12) for each produced nanopattern have been measured from SEM images of the patterns.

2.2 Bacterial experiments

2.2.1 Bacterial growth conditions

After production of the nanopatterned samples, they were seeded with gram-positive bacteria *Staphylococcus aureus* (*S. Aureus*) (RN0450 strain) (BEI Resources, VA, USA) in order to investigate their bactericidal effect. The procedure used was based on previous research [35].

Before this process could be applied, first *S. aureus* bacteria were cultured using Brain Heart Infusion (BHI) broth. Both a liquid and solid medium were used, where the liquid medium was produced using 37 grams of BHI broth powder (Fluka Analytical, BCBN2163V) in 1 litre of distilled water, while the solid medium was formed by using 52 grams of BHI agar (Fluka Analytical, BCBM2747V) in 1 litre of distilled water. After forming the solutions, both were then autoclaved for a duration of 20 minutes at 121°C. After the autoclaving the solid BHI agar was heated to become liquid phase and subsequently poured in a petri dish. Upon solidification of the BHI agar plate, the *S. aureus* from a frozen vial was streaked onto it. Next, the plate was incubated (Heraeus, Thermo) overnight at 37°C to allow the formation of discrete bacterial colonies.

The process of seeding the samples with *S. aureus* was then initiated by preparing a preculture of *S. aureus*. To do this, a single homogeneous colony was taken from the incubated BHI agar plate and inserted into a 10 mL solution of liquid BHI. This mixture was then incubated in a shaker-incubator (Innova 44, New Brunswick) at 140 RPM and 37°C for 18 hours. 18 hours was taken as the duration to ensure the bacterial cells were used before they went into the saturation stage of their growth cycle, see Appendix A1. After this incubation period the optical density (OD) of this solution was measured using absorption spectroscopy (using the *WPA Biowave II*) at a wavelength of 600 nm (OD_{600}), in order to allow for dilution of the mixture to an OD_{600} of 0.2. Before applying this dilution to the nanopatterned samples, the samples were first sterilized by submerging them in 70% ethanol and, after removing the ethanol, exposing them to UV-light for 20 minutes in a sterile flow cabinet. The samples were then placed in a 24-well plate (Cell Star, Germany) and prewet using 0.5 mL of liquid BHI. This prewetting step was applied to aid in the formation of a homogeneous bacterial distribution on the substrate surface. Afterwards, 0.5 mL of the 0.2 OD_{600} solution was introduced to these wells to form a final 0.1 OD_{600} *S. aureus* and liquid BHI mixture. By doing so, the sample was inoculated with 147.75×10^6 CFU (Appendix A2). To ensure homogeneous seeding, the well plate was then shaken at 100 RPM for 5 minutes (using the *IKA KS 260*). Finally, the well plate was placed in the incubator at 37°C for 18 hours. Figure 5 illustrates the process up until this point.

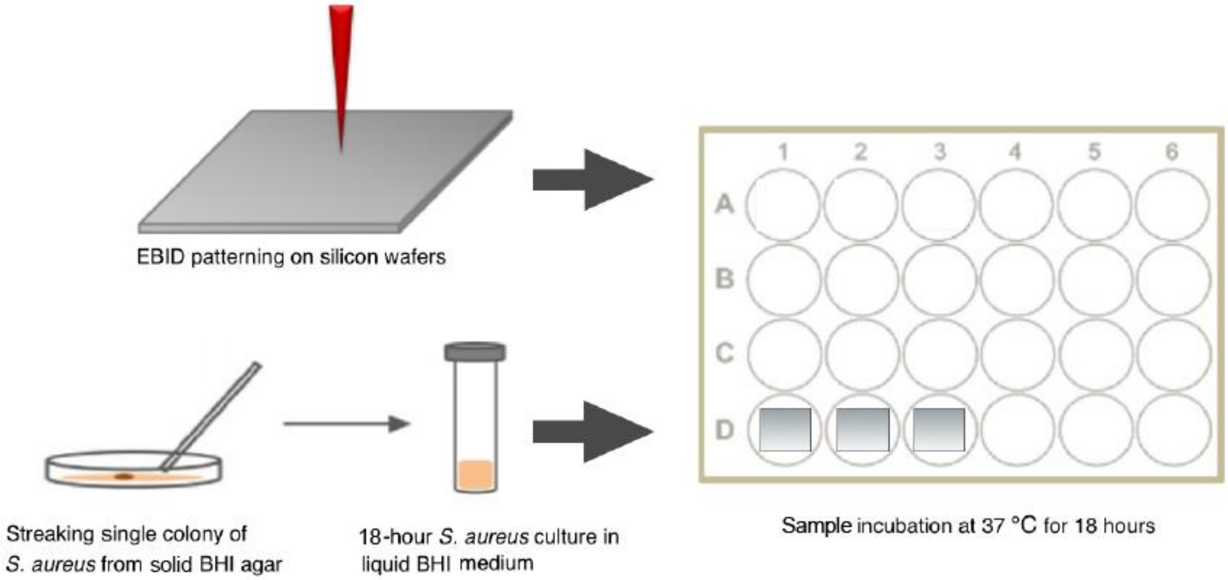

Figure 5. Schematic of the procedure for bacterial culturing. A culture of *S. aureus* is grown over 18 hours from a single colony in liquid Brain Heart Infusion (BHI). This culture is applied to silicon samples containing EBID-fabricated nanopatterns in a 24-well plate and subsequently incubated at 37°C for an 18 hour period. Image based on schematic by M. Ligeon (2018) [47].

Next, the morphological state of the bacteria had to be fixed to prevent them from moving or growing. This incapacitates them and allows for clear imaging of a time-frozen state of the bacteria on the substrate surface. Samples were first rinsed twice with 10 mM phosphate-buffered saline (PBS) to remove non-adherent bacteria. Next, 1 mL of fixation solution (consisting of 4% formaldehyde (Sigma-Aldrich, Missouri, USA) and 1% glutaraldehyde (Sigma-Aldrich, Missouri, USA) in PBS was applied to the bacteria-covered samples to freeze the morphological state of the bacteria. The samples were subsequently placed in a 4°C fridge for a duration of 1 hour, which duration was based on experiments performed regarding this fixation time (Appendix A3). Afterwards, the samples were dehydrated through a series of distilled water and ethanol washing steps. As evaporation occurs when high-concentration ethanol is applied to the bacteria-containing samples, which causes bacterial-aerosols to come free, the ethanol-washing was divided into steps. Working up from a low-concentration ethanol to a high-concentration ethanol, these steps apply MilliQ water and 50%, 70% and 96% ethanol respectively to the samples. The samples were then shaken for 5, 15, 20 and 20 minutes respectively to ensure the samples being completely submerged in the solutions. Each step used 1 mL of each solution and the shaker was set to 50 RPM. Next, to ensure every bit of water was extracted from the bacterial cells, the samples were soaked in 1 mL of hexamethyldisilazane (HMDS) (Sigma-Aldrich, MO, USA) for 30 minutes. Afterwards, the samples were air-dried.

2.2.2 SEM/FIB imaging and evaluation

Before being able to use SEM for imaging of the bacteria-covered samples, they were first covered in a thin layer of gold by gold-sputtering. SEM images were made of the bacteria-covered samples at different magnifications and at 0° and 52° tilt, both on and around the nanopatterns to be able to compare bacterial densities between the different regions. The images were used for manual counting of the number of bacteria adhered to the substrate surface in the different regions (to compare the bacterial density on the patterns to the density on flat areas, as to assess whether bacterial adhesion was inhibited more on the patterns), as well as for assessment of bacterial health.

The bacterial cells were categorized as either alive (healthy), deformed (deviating from the health state), or dead (heavily deformed or collapsed) based on their morphological state compared to a normal healthy cell or by observing cell-wall disruptions, as illustrated in Figure 6. Both the deformed and dead cells were considered damaged cells and these were counted for each pattern. By dividing the number of damaged bacteria by the total number of bacteria in each region, the bactericidal efficiencies of the nanopatterns were determined. This parameter could be formulated as follows:

$$bactericidal\ efficiency = \frac{damaged\ cells}{total\ number\ of\ cells}$$

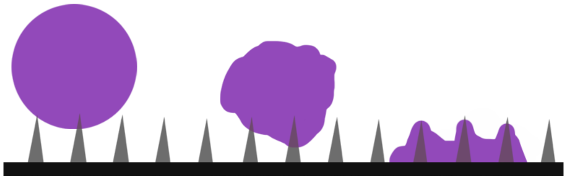

Figure 6. Illustration of the health of *Staphylococcus aureus* on a nanopillar pattern. Left to right: a healthy, deformed and dead bacterial cell.

To make a clear comparison between the bactericidal capabilities of each nanopatterns, multiple comparisons were made. Firstly, reproducibility of the bactericidal efficiencies of each pattern was tested. To do so, each sample was produced and tested twice. Secondly, the nanopatterns without disorder were compared to each other, to assess the influence of interspace on the bactericidal effect of ordered patterns. Thirdly, the nanopatterns without disorder were compared to their disorder-containing counterparts, to assess the influence of disorder on the bactericidal effect.

In order to investigate the interaction between the bacterial cells and the nanopillars and to analyse the killing mechanism, focused ion beam scanning electron microscopy (FIB-SEM) experiments were performed in a FIB microscope (FEI, Helios G4 CX dual beam workstation, Hillsborough, OR, USA). The sample was tilted to 52°, a layer of platinum was deposited over the area of interest (a 2.43 × 0.97 μm^2 area, with $Z = 1$ µm) using ion beam, the surface was then milled with a 7 pA ion beam ($Z = 1.5$ µm).

2.2.6 Statistical analysis

Statistical analyses have been performed using IBM SPSS Statistics 23 Software. The analyses were performed to assess the level of significance in observed differences between the bactericidal efficiencies of different patterns, as well as the significant differences between bacterial densities on patterned and non-patterned areas. The significance was calculated using Mann-Whitney U tests. To perform these statistical analyses, the mean ± standard deviation values of the bacterial measurements were used. Significance levels that were considered were $p < 0.05$ (denoted *), $p < 0.01$ (denoted **), $p < 0.001$ (denoted ***) and $p > 0.05$ (denoted “n.s.” or omitted).

3. Results

3.1 Characterization of the nanopatterns

SEM images of the patterns at different magnifications and stage tilt angles are shown in Figures 7a-c and 8a-c, which display the ordered and disordered patterns respectively. To further visualize the 3D overview of the nanopatterns, AFM images of the patterns are displayed in Figures 7d and 8d. SEM images providing an overview of the full 20 × 20 μm^2 nanopatterned areas have been included in Appendix A8. Table 3 contains an overview of the nanopillar heights, base diameters and pillar densities. The nanopattern with the smallest interspace was the 100 nm interspace, 0 nm disorder pattern. At this interspace, it can be seen that pillars are very close together, experiencing a strong influence from the proximity effect, which broadens their diameters. At 170 nm interspace, pillars are close enough together to still experience the proximity effect, again broadening their diameters. Figure 8 shows that due to the small interspace combined with the disorder distance, pillars are more likely to cluster together and form high density local areas. At 300 nm interspace the pillars are spaced far enough from each other to not experience a significant influence of the proximity effect, meaning the pillar diameters get smaller. To account for this, extra dwell time was used in combination with applying a focus blur. At 500 nm interspace pillars are spaced far apart. No difference in influence of the proximity effect was observed relative to the 300 nm interspace patterns. From the 500 nm interspace AFM image in Figure 7d the actual dimensions of the nanopillars could be measured, showing the pillar interspacing and heights did seem to conform to the designed values. Due to the geometry of the AFM tip the pillar diameters could not be measured representatively.

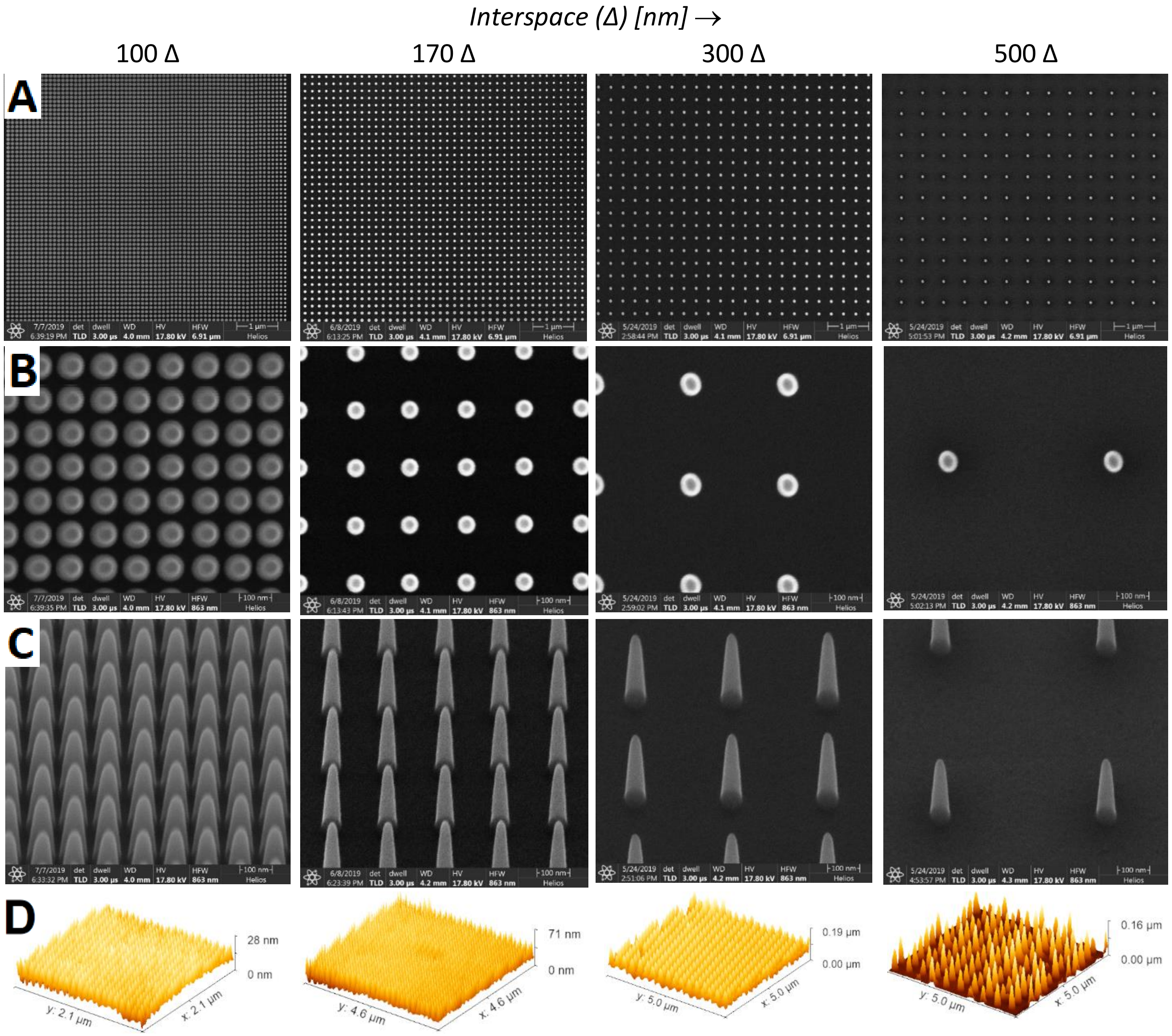

Figure 7. SEM images of the 20 × 20 μm^2 ordered nanopatterns with different interspaces (Δ), at different magnifications. **A.** An overview of one of the nanopattern arrays, at a horizontal field width (HFW) of 6.91 μm. **B, C.** The array at 0° tilt and 52° tilt, both taken at HFW 863 nm. **D.** AFM images showing the 3D overview of the nanopillar patterns.

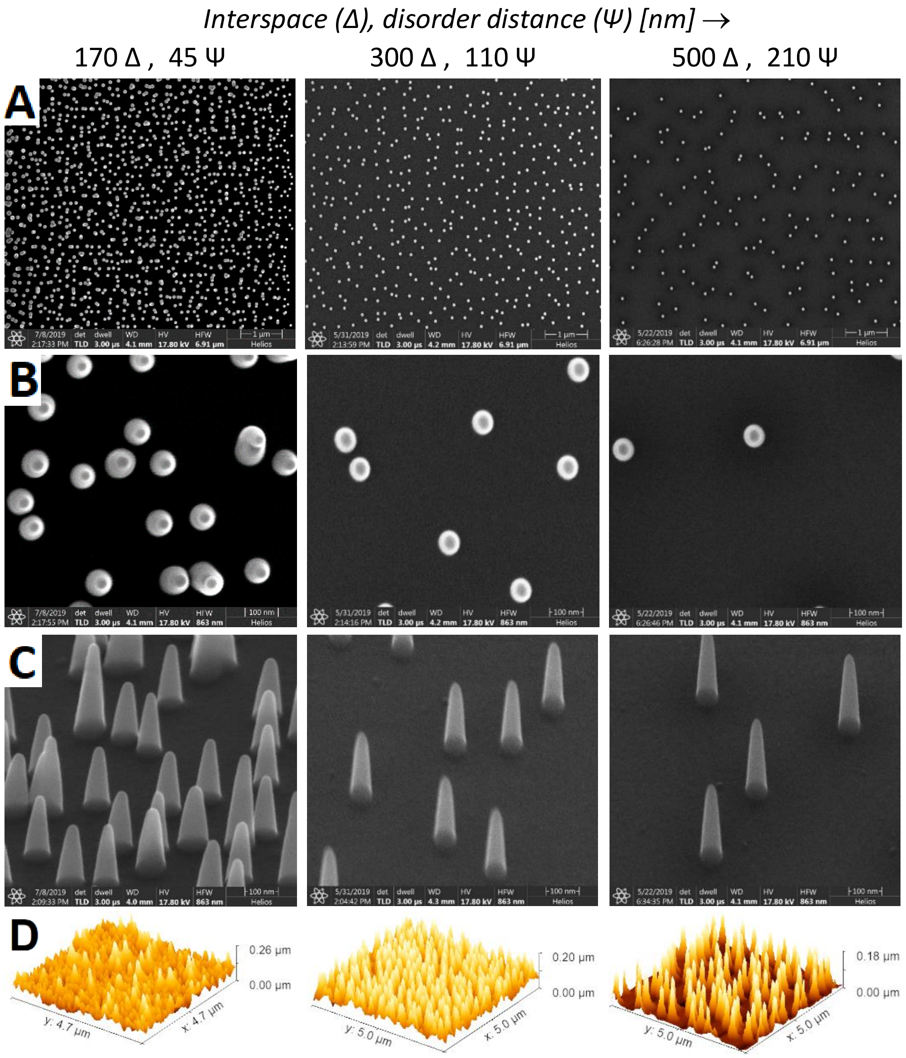

Figure 8. SEM images of the 20 × 20 µm^2 nanopatterns with different interspaces (Δ) and maximum disorder distances (Ψ), at different magnifications. **A.** An overview of one of the nanopattern arrays, at HFW 6.91 µm. **B, C.** The array at 0° tilt and 52° tilt, both taken at a horizontal field width (HFW) of 863 nm. **D.** AFM images showing the 3D overview of the nanopillar patterns. For the 500 Δ pattern some pillars were damaged due to a too high applied AFM force.

The pillar dimensions (height and base diameter) were measured from these SEM images. These dimensions are displayed in Figures 9 and 10 respectively. As can be seen, the dimensions were quite variant. The mean diameters often deviate about 10 nm from the preferred diameter of 80 nm. The nanopillar heights also deviate a maximum of several tens of nanometres from the preferred height of 180 nm. The mean heights and diameters are also shown in Table 3.

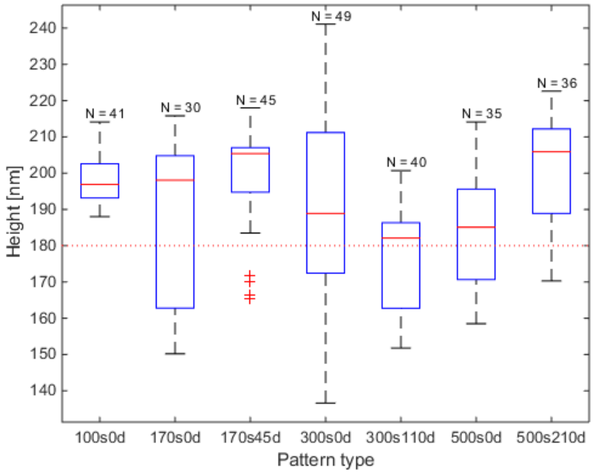

Figure 9. Pillar heights of the nanopatterns as determined from SEM images, both with and without disorder. Sample sizes (N = number of measured pillars) have been included. A horizontal line marks the designed height (180 nm).

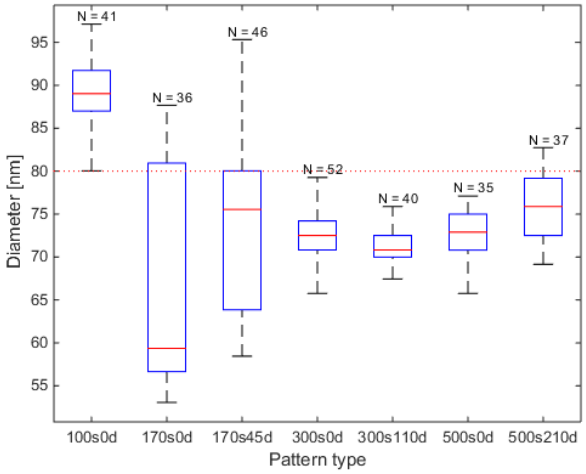

Figure 10. Pillar base diameters of the nanopatterns as determined from SEM images, both with and without disorder. Sample sizes (N = number of measured pillars) have been included. A horizontal line marks the designed diameter (80 nm).

Additional parameters that were determined for the fabricated nanopatterns were their chemical composition, pillar density and contact angle. The nanopatterns have a chemical composition including ≈15.5% Pt, ≈73.4% C, and ≈8.7% O [35]. The water contact angle measurement on the surface of Pt-C from previous research showed the surface was hydrophilic with a contact angle θ_0 of 59 ± 2° [35], which was used to estimate the wettability of the nanopatterns in this report. The tip diameters that were measured for each nanopattern are shown in Table 3, together with the calculated contact angles. From these contact angles the hydrophobicity of the nanopatterned surfaces is shown [48]. Table 3 also contains the pillar densities. For the disordered patterns the average pillar density is the same as that of the ordered pattern with the same interspace. However, due to the random displacement of the pillars, there are areas within an array with higher and lower local pillar densities.

Table 3*: Nanopillar height, base diameter, tip diameter, density and contact angle per nanopattern design. The pillar heights and diameters are mean values determined from SEM images.*

Interspace (Δ) [nm]	Disorder distance (Ψ) [nm]	Height [nm]	Base diameter [nm]	Tip diameter [nm]	Pillar density [number/μm²]	Contact angle [°]
100	0	197.9 ± 7.3	88.9 ± 4.2	31.2 ± 2.1	100.6	152 ± 2
170	0	187.8 ± 21.8	67.4 ± 12.6	20.9 ± 5.3	35.5	169 ± 3
170	45	199.8 ± 12.7	72.9 ± 9.3	23.6 ± 2.1	35.5	168 ± 1
300	0	189.5 ± 28.2	72.6 ± 3.1	22.7 ± 2.8	11.9	173 ± 1
300	110	177.2 ± 13.5	71.3 ± 1.9	20.9 ± 3.6	11.9	174 ± 1
500	0	184.3 ± 15.9	72.3 ± 2.8	20.0 ± 3.6	4.5	177 ± 1
500	210	200.8 ± 14.8	75.9 ± 3.8	21.8 ± 2.5	4.5	176 ± 1

3.2 Bactericidal effect of the nanopatterns

3.2.1 Effect of interspace

The ordered nanopatterns were compared to each other to examine the effect of interspace on the bactericidal efficiencies of nanopatterns. SEM images of bacteria-covered nanopatterned 20 × 20 μm^2 areas per nanopattern design are shown in Figure 11. From these images the bacterial densities and bactericidal efficiencies were determined by counting the number of healthy, deformed and dead cells (also included in Appendix A4, Table 4). It can be seen that there were bacteria both on and around the patterned areas. The bacterial densities of the flat, non-patterned areas surrounding the patterns were compared to the bacterial densities on the patterns. This was done to compare bacterial adhesion between the patterned and non-patterned areas, which showed no significant differences (Figure 12). Note that the number of bacteria itself is no indication of the bactericidal efficiency, as the number of bacteria was not constant per experiment. The experiments were performed in duplicate and no significant difference was observed between the results of the two experiments.

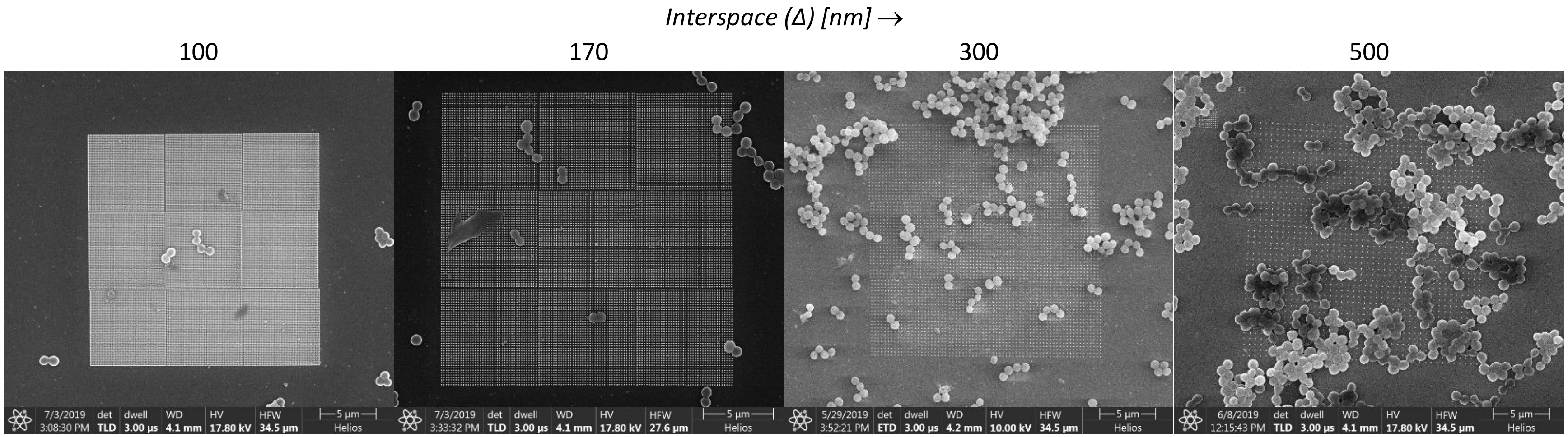

Figure 11. *Staphylococcus aureus* bacteria on 20 × 20 µm^2 ordered nanopatterns consisting of nanopillars with varying interspace distances. The number of healthy, deformed and dead bacteria were counted and from this the bactericidal efficiencies were calculated.

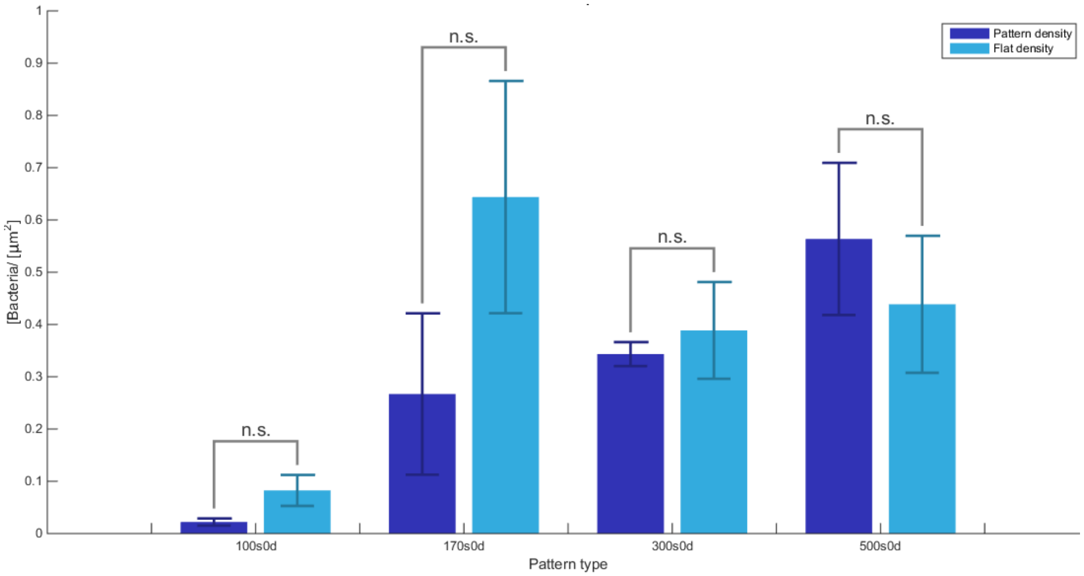

Figure 12. Bacterial densities on flat, non-patterned areas compared to the densities on the ordered patterned areas. Densities were calculated by counting the total number of bacteria in a 20 × 20 µm^2 area from SEM images. Sample sizes (N = number of bacterial cells) have been included.

The bactericidal efficiencies of the nanopatterns were compared with respect to the interspaces of the patterns (Figure 13a). These numbers amount to average bactericidal efficiencies of 62.3 ± 23.1%, 45.0 ± 31.4%, 8.6 ± 4.2% and 3.7 ± 2.3% for the 100, 170, 300 and 500 nm interspace samples respectively. From this, significant differences were observed between the different interspaces, the trend indicating higher bacterial efficiencies when the interspace becomes smaller. Figure 13b shows a SEM image of healthy and damaged bacterial cells on a 300 nm interspacing sample.

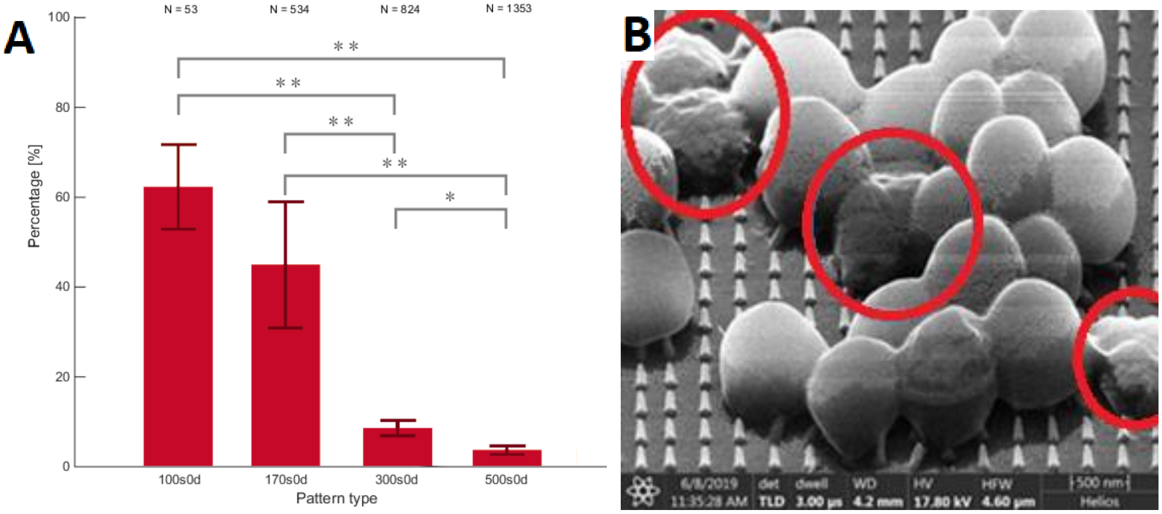

Figure 13. **A.** Effect of interspace on bactericidal efficiencies of ordered nanopatterns. The nanopatterns have 100 nm, 170 nm, 300 nm and 500 nm interpillar spacings (Δ) and efficiencies have been calculated through counting healthy, deformed and dead bacteria from SEM images. Sample sizes (N = number of bacterial cells) have been included. Significance levels given are $p > 0.05$ (omitted), $p < 0.05$ (*), $p < 0.01$ (denoted **). **B.** SEM image of *S. aureus* bacteria on a 300 nm interspace nanopattern. Damaged bacteria have been circled, where deformation is clearly indicated by the disrupted morphology, forming rippled cell walls in contrast to the smooth wall of the healthy cells.

3.2.2 Effect of controlled disorder

The ordered and disordered nanopatterns were compared to each other regarding their bactericidal efficiencies to examine the effect of controlled disorder on the bactericidal efficiency of nanopatterns. SEM images of bacteria-covered nanopatterned 20 × 20 μm^2 areas per disordered nanopattern design are shown in Figure 14. For each of the interspace-variant patterns with disorder, the number of healthy, deformed and dead cells observed were counted (also included in Appendix A4, Table 5). Bacteria were seen both on and around the patterned areas. The bacterial densities of the flat, non-patterned areas surrounding the patterns were compared to the bacterial densities on the patterns. This was done to compare bacterial adhesion between the patterned and non-patterned areas, which showed no significant differences (Figure 15). Again, the bacterial density on each pattern is no indication of the bactericidal efficiency.

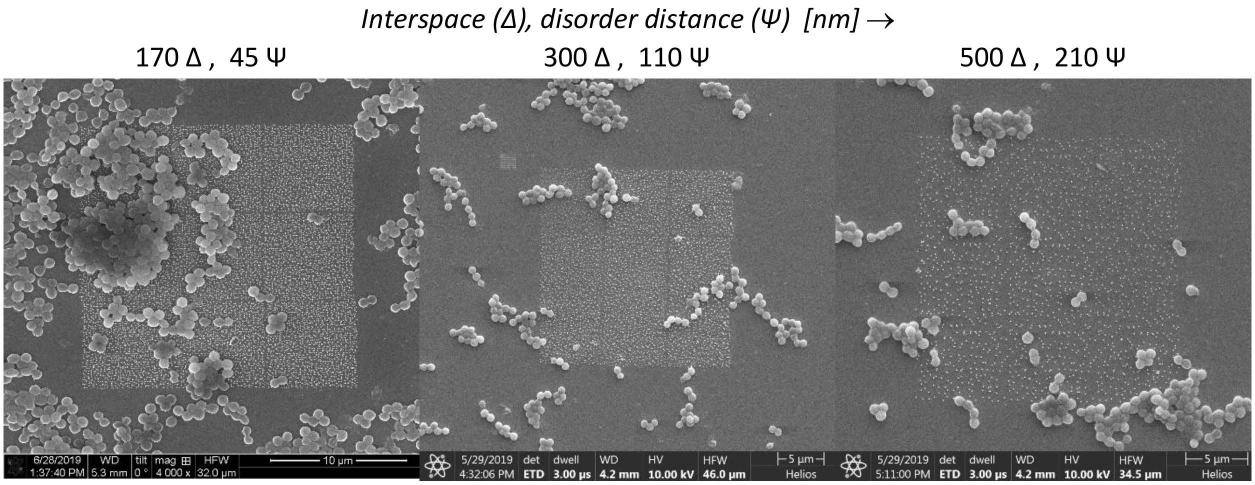

Figure 14. *Staphylococcus aureus* bacteria on 20 × 20 µm^2 disordered nanopatterns consisting of nanopillars with varying interspace distances. The number of healthy, deformed and dead bacteria were counted and from this the bactericidal efficiencies were calculated.

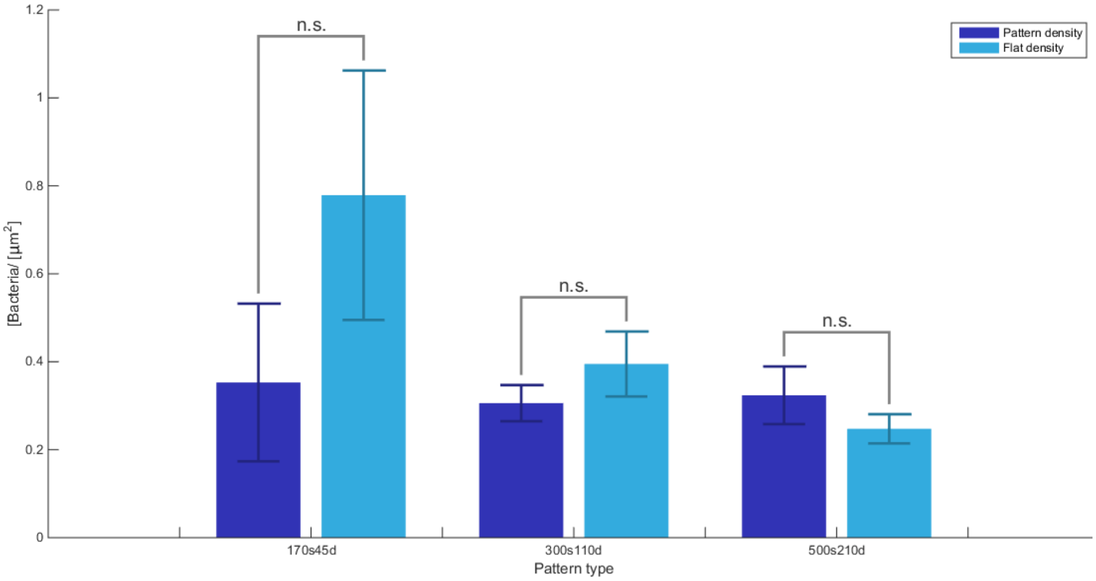

Figure 15. Bacterial densities on flat, non-patterned areas compared to the densities on the disordered patterned areas. Densities were calculated by counting the total number of bacteria in a 20 × 20 µm^2 area from SEM images. Sample sizes (N = number of bacterial cells) have been included.

The average bactericidal efficiencies of the disordered nanopatterns were 45.9 ± 29.2%, 14.7 ± 7.2% and 12.7 ± 9.8% for the 170, 300 and 500 nm interspace samples respectively. The bactericidal efficiencies of the ordered and disordered nanopatterns have been compared to each other with respect to their interspace (Figure 16a). By doing so, a comparison could be made between the bactericidal performance of ordered and disordered patterns. As the 100 nm interspace sample had no disordered version, it was not included in this comparison. No significant difference was observed between the bactericidal efficiency of ordered nanopatterns with respect to disordered nanopatterns. Figure 16b shows a SEM image of healthy and damaged bacterial cells on a 300 nm interspace sample.

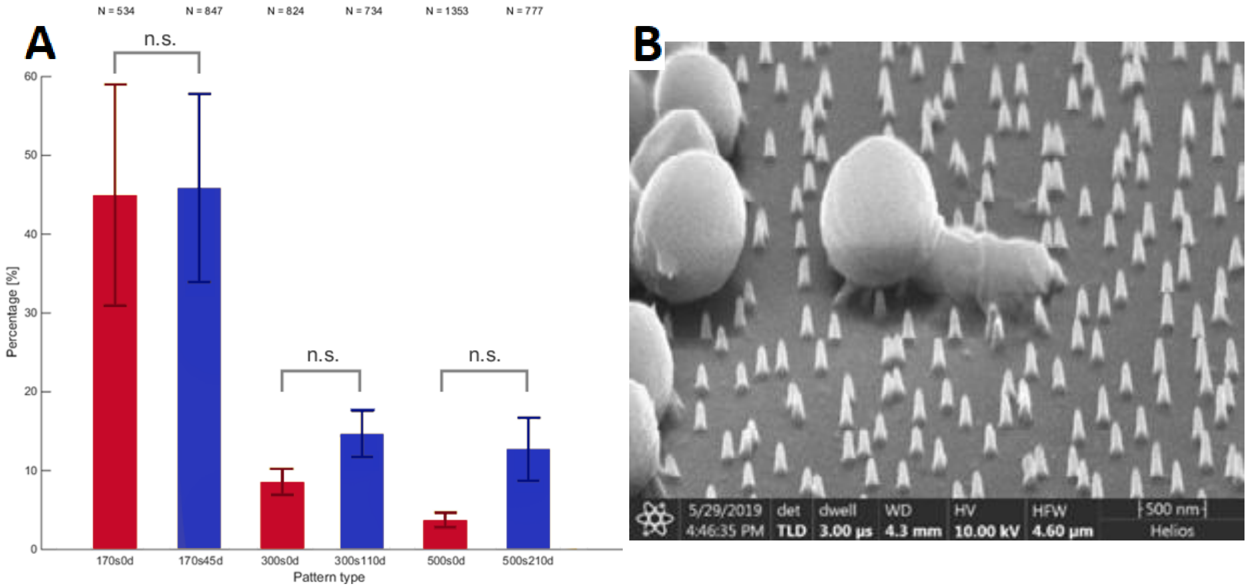

Figure 16. **A.** Effect of disorder on bactericidal efficiencies nanopatterns by comparing ordered and disordered nanopattern efficiencies. The nanopatterns have 170 nm, 300 nm and 500 nm interpillar spacings (Δ). Efficiencies have been calculated through counting healthy, deformed and dead bacteria from SEM images. Sample sizes (N = number of bacterial cells) have been included. **B.** SEM image of *S. aureus* bacteria on a 300 nm interspace nanopattern with disorder. A damaged bacterial cell is seen next to healthy bacterial cells, where deformation is clearly indicated by the disrupted morphology, forming rippled cell walls in contrast to the smooth wall of the healthy cells.

An overview of the effect the interspace distance has on the bactericidal efficiency of the ordered and disordered nanopatterns is shown in Figure 17. The trend of higher bactericidal efficiencies at lower interspace distances, which was observed for ordered nanopatterns, was also seen for the disordered nanopatterns.

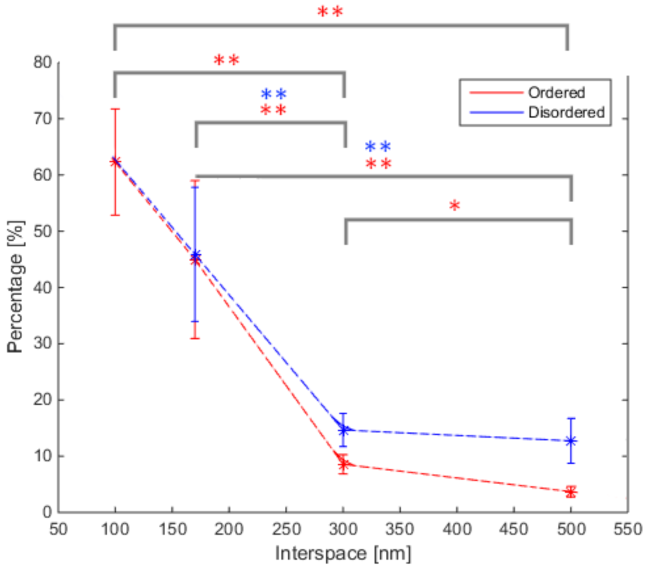

Figure 17. Trends of bactericidal efficiencies of ordered and disordered nanopatterns compared to the interspace distance (Δ). Significant differences have been denoted for both the ordered (red) and disordered (blue) patterns, significance levels given as p > 0.05 (omitted), p < 0.05 (*), p < 0.01 (denoted **).

3.2.3 FIB analysis of cell/pattern interface

The possible mechanisms behind the observed bactericidal effect of the nanopatterns were examined using focused ion beam (FIB). Cross-sections of one of the ordered 300 nm interspace samples were created to observe the interface between the *S. aureus* bacteria and the nanopillars (Figure 18).

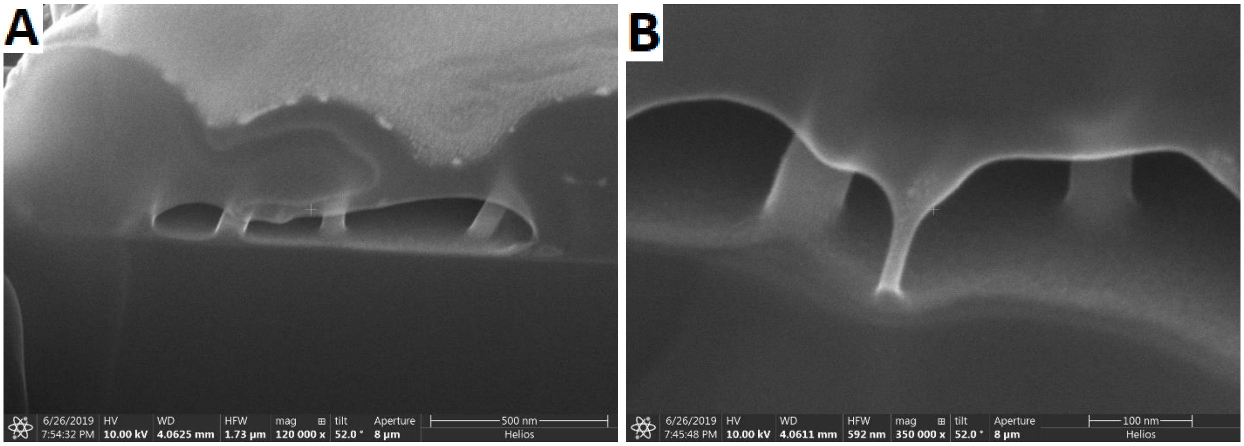

Figure 18. Focused ion beam (FIB) images of the interface between *S. aureus* bacteria and nanopillars of a 300 nm interspace ordered nanopattern. **A.** Cross-section of bacteria covered with a 1 µm platinum layer, nanopillars visible through the bacterial walls. The nanopillars seem to bend inwards into the bacterial cell. **B.** Higher magnification image, demonstrating pillar penetration of the cell wall.

4. Discussion

The aim of this research was to investigate effect of interspace and disorder of nanopatterns on their bactericidal efficiency. Significantly higher efficiencies were observed for patterns with lower interspacing, but no real significant difference was found between the ordered and disordered pattern bactericidal efficiencies. Combining these results with data available in literature helps provide more insight into the effect these parameters have on the bactericidal efficiency of nanopatterns.

4.1 Bactericidal mechanisms

According to previous research, it is believed three different mechanisms aid in the killing of the bacteria: cell rupturing by penetration of the cell wall; mechanotransduction pathways in which the bacterial genomics and metabolisms are affected by mechanical forces; extracellular polymeric substance (EPS) mediated cell membrane damage, where the bacteria attempting to move away from the nanopillars causes cell membrane damage (Figure 19) [24].

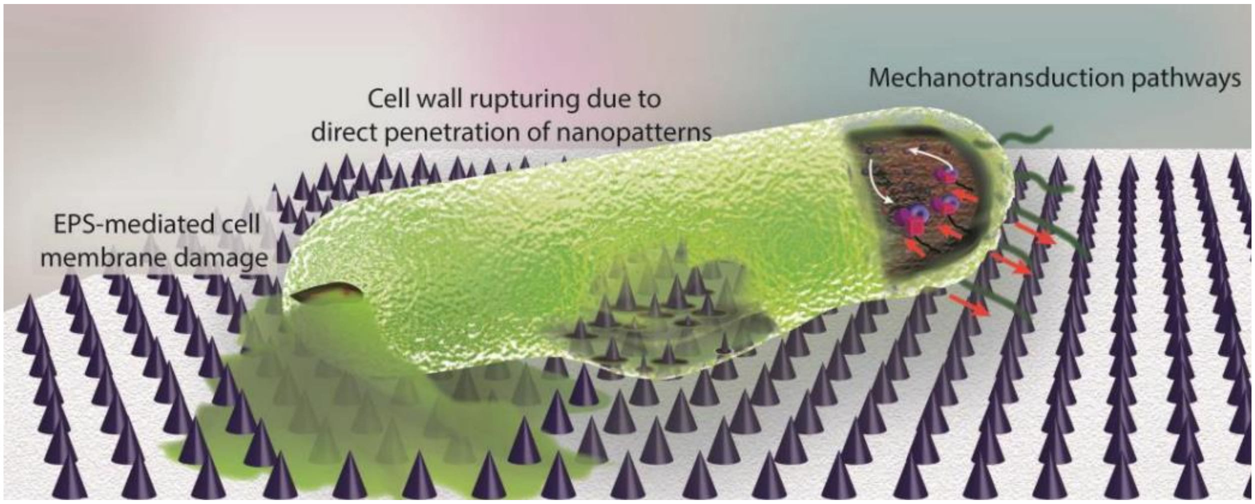

Figure 19. Main bactericidal mechanisms of nanopatterns. Commonly, cell wall rupturing is believed to cause cell death. Other studies suggest extracellular polymeric substance (EPS) plays a key role, causing cell membrane damage when the bacterial cell attempts to move away from the nanopatterned surface to a less rough surface. Lastly, mechanotransduction pathways in which the genomics and metabolomics of the bacteria are affected by mechanical forces could also cause bacterial death on the nanopatterned surface [24].

Finger-like extensions were observed protruding from the bacterial cells towards the tips of proximal nanopillars (Figure 20) and towards the sample surface (Figure 18b), seemingly stretching to aid in attaching. It can also be seen that the nanopillars appear to be bent in contact with the bacterial cells, supposedly from the pressure exerted upon them. The same effect has been found in previous research and literature [25, 38], however it is not clear whether indeed EPS-mediated cell membrane damage plays a role in killing the bacteria. In addition, Figure 20 also shows that the nanopillars tend to bend inwards into the bacterial cell wall, seemingly penetrating the cell wall or at least causing severe deformation from the "healthy" morphology of the bacteria. Although the nanopillars sometimes bend strongly, it does not seem to break them or detach them from the surface. This may indicate that indeed direct cell penetration aids in the killing of bacteria.

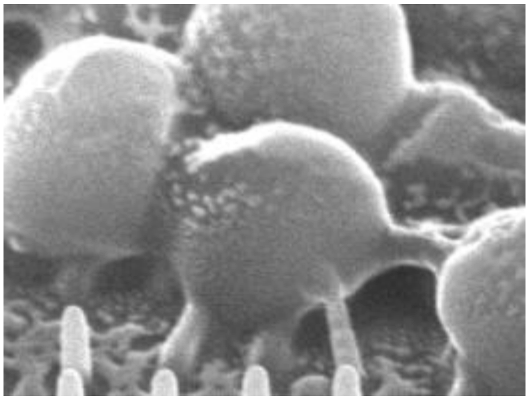

Figure 20. FIB image of extracellular polymeric substance (EPS) formation between the *S. aureus* bacteria and finger-like extension protruding towards the nanopillars. Nanopillars in contact with the bacterial cells appear to be bent under the pressure.

The nanopatterned areas that were designed in this work seem to show significant differences in bactericidal efficiency compared to each other. When comparing the effect of interspace distance on the bactericidal efficiency of the nanopatterns, the results showed higher bactericidal efficiencies at lower interspace distances (Figure 13a). Comparing the smallest interspace sample (100 nm interspace) with the largest interspace sample (500 nm interspace), a clearly significant difference in bactericidal efficiencies is seen ($p < 0.01$). This indicates there is indeed a prominent dependence of bactericidal efficacy on interpillar distance. Between the 100 and 170 nm interspace samples there is no significant difference in efficiencies due to the large variances. However, the 100 nm interspace sample does show a 17.3% percent higher average bactericidal efficiency. It can be seen that there is also a significant difference ($p < 0.05$) between the bactericidal efficiency of the 300 and 500 nm interspace samples. This shows that even though these efficiencies are relatively low compared to those achieved with the 100 and 170 nm interspace samples, the interspace still has a significant impact on the bactericidal potency of nanopatterns. With regards to bacterial densities on the patterns and on the flat areas, it seems there is no significant difference between them (Figure 13). As the bacterial densities on the flat areas also differ per sample, it seems the density differences are caused by other factors (such as bacterial growth procedure variances) rather than by the nanopattern interspace. At most the average bacterial density does seem higher on the flat areas than that of the patterned areas, meaning there could still be a small amount of bacterial adhesion prevention. Only for the 500 nm interspace pattern this does not hold, possibly indicating nanopatterns with that interspace actually promote bacterial adhesion, instead of preventing it.

At the lowest interspace distance of 100 nm, the achieved bactericidal efficiency (62.3 ± 23.1%) appears reasonable with regards to the suspected influence of interspace on the bactericidal properties of nanopatterns (increasing the number of contact points with the bacterial cells). In literature, comparable nanopatterns with pillar diameters of 80.3 nm, heights of 432.5 ± 63.5 nm and interspace of 99.5 nm were able to kill 73% of *S. aureus* bacteria [44]. Other literature, however, reported a 23-31% bactericidal efficiency for patterns with an interspace of 130 nm, pillar diameters of 80 nm and heights of 200-250 nm [46], which pillar dimensions are more in the range of those used in our study. Due to this, it was hypothesized that larger pillar heights would be needed to increase bactericidal effects of patterns with low interspace distances. However, as this research has shown it seems this is not necessary, as the produced 180 nm height and 80 nm diameter nanopillars performed well. This possibly indicates that the effect of pillar height on bactericidal efficiency is not as significant as the effect of pillar interspacing, as was also hypothesized in other literature based on computer simulations [49]. The average bactericidal efficiency found for the 170 nm interspace pattern (45.0 ± 31.4%) is comparable to the one found in previous research (36 ± 5%) [35]. This confirms the reproducibility of those results and at least confirming the validity of the 170 nm interspace sample results obtained in this research. In another study, patterns with an interspace distance larger than 300 nm and nanopillar height of 150 nm demonstrated a 31% bactericidal effect on *S. aureus* [46], which differs significantly from the 8.6 ± 4.2% bactericidal efficiency found in this research. That study, however, made use of live/dead staining to assess the health of the bacterial cells, which is a more accurate method than the visual assessment used in this research. This is due to the fact that not every deformed/dead cell changes its morphology, which hinders visual assessment. However, the same study also achieved a 98% bactericidal efficiency for 170 nm interspace nanopatterns with 200 nm pillar height, which also differs significantly from our obtained values. With regards to the 500 nm interspace nanopattern, the low bactericidal efficiency (3.7 ± 2.3%) seems to be in trend with the relation between interspace and bactericidal efficiency presented in this study. Other literature did not provide information on the effect of this interspace distance, as interspace values reported for bactericidal nanopatterns usually are in the range of 150-300 nm [45].

With regards to the effect of controlled disorder on the bactericidal efficiency, it seems disordered nanopatterns generally perform slightly better than ordered nanopatterns (Figure 16a, 17), however non-significantly for each of the patterns. In general, no significant difference is observed between the ordered and disordered pattern, except for a slightly higher bactericidal efficiency of the disordered nanopatterns. The pillars clustering together due to the random disorder cause local higher pillar densities, which may cause slightly higher bactericidal potencies due to the increased amount of contact points with the bacteria in those areas. If true, this would have the beneficial effect of being able to use relatively less pillars (higher interspace) while still exhibiting higher bactericidal efficiencies than when no disorder would be introduced to their arrangement. The benefit of this is the reduced fabrication time needed to produce these patterns, which for the relatively slow EBID process (170 nm/s production speeds [31]) is a welcome addition. Overall, for both the ordered and disordered patterns, the trends (Figure 17) seem to show higher bactericidal efficiencies at lower interspace distances. As with the ordered nanopatterns, no significant difference is observed between the patterned and non-patterned areas with regards to their bacterial densities (Figure 15). However, comparing the difference between the average bacterial density on and off the patterns shows that there was a larger difference (0.43 μm^{-2}) for the 170 nm interspace sample than with the 300 nm (0.09 μm^{-2}) and 500 nm (0.08 μm^{-2}) interspace samples. This may indicate the lower interspace distance had a stronger effect on preventing bacterial adherence.

Information in other literature on the effect of disorder on bactericidal efficiency is minimal. It was only found that nanopatterns with pillars of 150-200 nm in diameter and 100-250 nm interspacing were produced based on wings of different insects, which were able to kill $2.2*10^5$ cell/h per cm^2 of *S. aureus* [50]. No percentage was provided in that article, however, which makes it hard to relate to this research. Other research fabricated nanopatterns with 300 nm interspace, 122 ± 22 nm pillar diameters and 183 ± 9 nm pillar heights, both with 0 and 50 nm disorder [25]. The bactericidal efficiencies of the ordered and disordered patterns on *E. coli* were compared, showing no significant difference. It was thus concluded that the controlled disorder did not adversely affect the bactericidal efficiency on *E. coli*, while the same controlled disorder was known to be beneficial to osteogenic differentiation of mesenchymal stem cells (MSCs) as opposed to ordered patterns. In this research, however, it can be seen that for *S. aureus* there does seem to be a better bactericidal effect for the 300 nm interspace disordered patterns than the ordered patterns, although non-significantly (Figure 16). This could indicate that indeed such nanopatterns are both bactericidal and osteogenic, which is a very valuable characteristic for use in countering IAIs. In general, the trends in Figure 17 seem to indicate the best antibacterial performances at lower interspace distances. This trend is not expected to continue towards lower interspace distances (at these pillar dimensions) however, as reducing the interspace distance further would effectively increase the contact area between *S. aureus* bacteria and the nanopattern to such an extent that the nanopattern almost forms a flat (slightly rough) surface [49]. This is counter-effective due to the total free energy gain increasing with contact area (reducing stresses exerted on the bacterial cell), while surfaces with high roughness cause the bacterial cells to be suspended between the pillars and decrease free energy gain with several orders of magnitude (Figure 21) [51]. This means stronger bacterial adhesion will occur on surfaces with lower roughness and pillar density.

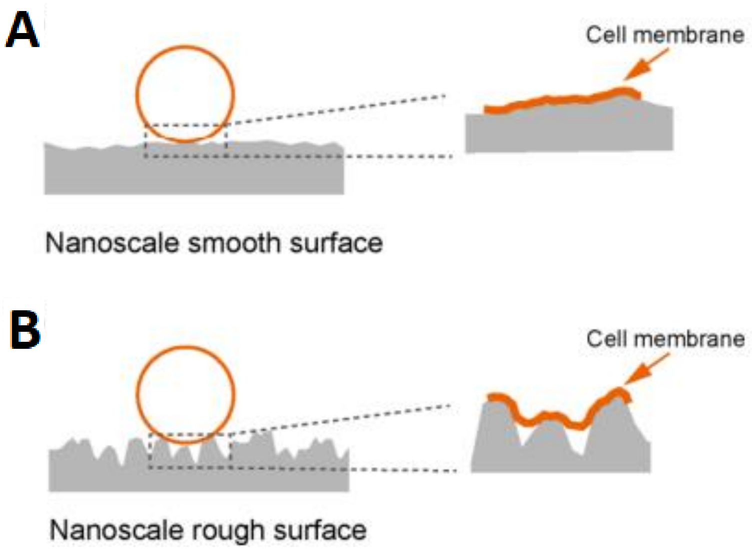

Figure 21. Schematic of bacterial adhesion with regards to surface roughness. **A.** Smooth surface, causing high adhesion. **B.** Rough surface, bacterial cell is suspended between pillars, which causes low adhesion [51].

Additionally, disordered patterns seem to perform on average 5.4% better at damaging bacteria than ordered patterns. Both these improvements to bactericidal efficiencies (smaller interspace and introduction of disorder) could be explained by the pillar density of the nanopatterns. As the pillar density is the amount of pillars per µm^2, this parameter is directly related to the number of contact points with the bacteria. To illustrate, the difference between bactericidal performance against *E. coli* and *S. aureus* (97 ± 1% and 36 ± 5% respectively) from previous research [35] could be examined with respect to pillar density. *E. coli* bacteria are rod-like 2 µm long, 0.25-1 µm in diameter (~0.5-2 µm^2 contact area), while *S. aureus* bacteria have a 0.6 µm cell diameter and are much more spherical (~0.28 µm^2 cross section surface area) [45]. This means with a 170 nm interspace nanopattern, which has a pillar density of 35.5 µm^{-2}, *E. coli* has a minimum of ~17.75 contact points. In contrast, *S. aureus* would have only ~9.94 contact points when assuming *S. aureus* has a flat bottom (cross section). Since *S. aureus* does not have a really flat bottom, the number of contact points is even smaller. Theoretically, this means that to exert the same level of stress on *S. aureus* bacteria as on *E. coli* bacteria, the pillar density would need to be increased, which has also been theorized in other literature [49]. As is shown in Figure 12a, it seems this theory does hold, as a reduction in interspace distance effectively increased pillar density and by doing so increased the bactericidal efficiency.

4.2 Limitations

A factor that could have influenced the bactericidal efficiencies is the pillar dimensions. As is shown in Figure 9, 10, the nanopatterns that were produced showed some variance with respect to each other. As was noted before, other research has found that the height of nanopillars is not as influential to the bactericidal capabilities of the nanopatterns as the combination of pillar diameter and interspace is [49]. As of such, the deviations in pillar height shown in Figure 9 are not expected to have caused large changes to the bactericidal efficiencies of the nanopatterns. The deviations in Figure 10, however, could have had some influence, as the relatively low pillar diameters of the 170 nm interspace ordered and disordered patterns (first experiment) effectively increase the distance between pillars and thereby the effective interspace. Statistical analysis, however, indicated no significant difference between the two experiments of those patterns, meaning it is not clear whether the diameter deviations could have caused a large change from the "true" bactericidal efficiency. Comparing the pillar dimensions in the AFM images (Figure 7d, 8d) to the SEM images shows a slight difference due to different measurement accuracies, as SEM measurements are generally less accurate than those performed by AFM. This means the large variances could have been partly caused by inaccurate measurements.

The large standard deviations that were obtained indicate a significant variability was present in the final results, possibly caused by "washing off" healthy bacteria during the bacterial procedure. For some experiments, it was observed that after applying the PBS solution to the samples, a white "plaque" was loosened from the sample surface and suspended in the solution. After SEM imaging the sample surface, the significantly lower bacterial density that was observed showed this white plaque was possibly a large amount of bacteria. Due to this, the results may have been inaccurate, as it is possible relatively more healthy than deformed/dead bacteria were washed off. As can be seen in Appendix A4, bactericidal efficiencies of 100% (0 healthy bacteria) were obtained mostly for patterns with low bacterial densities (low sample sizes), possibly indicating those were instances at which bacteria were washed off. If the bacterial density was higher and thus the amount of deformed/dead bacteria was higher as well, a bactericidal efficiency of 100% would have been more reasonable to accept. The difference in bacterial densities per bacterial culture are believed to be caused by variations in the state of the bacteria in the preculture. As Figure 23 (Appendix A1) shows, a different growth rate was observed than in previous research [35]. This difference may have been due to the preculture bacteria being in a different growth state with respect to those in previous research, which causes more bacteria on the samples than expected. Besides the washing off of bacteria, another factor was believed to have influenced the amount of bacteria present on the nanopatterned areas. This factor was bacteria moving away from the patterned area in favour of less rough or flat (nonpatterned) areas, suspected due to the presence of remnant *S. aureus* fragments on the nanopatterns [35]. Figures 13 and 16 show the bacterial densities on non-patterned areas compared to those on patterned areas, which have shown no significant differences. This may indicate that the bacteria do not actually move away in significant amounts or significant distances from the surface as was speculated in previous research, meaning the bacteria on the nanopatterned areas are mostly unable to escape. The remnant fragments, which were also found during the experiments performed in this research, may simply be caused by the washing off of the bacteria, leaving behind ruptured bacterial fragments (possibly from secreted EPS). It is to be noted that the non-significant difference in bacterial densities of flat and patterned areas is not necessarily negative. This is because in other research it has been suggested that allowing bacterial adherence to a nanostructured surface and subsequently killing them physically could be more effective for bactericidal surface design than by simply repelling the bacteria from the surface [45].

4.3 Further research

In order to achieve more accurate results, several steps of the process could be refined if needed. To reduce the variance of the nanopillar dimensions, more time should be spent on perfecting the parameters values used per nanopattern design. In addition, the total patterned area of 20 × 20 µm^2 could be enlarged to increase the sample size. As the bacterial distribution on the samples was not entirely homogeneous, upscaling of the nanopatterned area would include more differently distributed parts of the bacterial culture and therefore result in a more accurate measurement of bactericidal efficiencies over a larger area. Not only this, but larger patterned areas are also necessary to perform experiment using mammalian cells such as MSCs [35]. However, as was stated before, upscaling using EBID is difficult due to it being an inherently slow, small scale process (Table 2) [30]. This means other methods should be added or substituted to the process used in this research. One available option is the use of a multibeam scanning electron microscope, which enables parallel EBID and could significantly increase the fabrication speeds by using e.g. 14 × 14 beams [52]. Another option is to use nanoimprint lithography (NIL), which is a process that can use an EBID produced pattern as a mask stamp for rapid repeated fabrication of the same pattern. Using NIL, the total nanopatterned area can be increased at a high pace to cover areas of for example 3 × 3 mm^2 [35].

In the current research, visual assessment of bacterial cell health was used as the primary method of determining the bactericidal efficiencies of the nanopatterns. In future research, to the end of more accurately determining bactericidal efficiencies, a method such as live/dead staining could be used as the primary assessment method, as the staining process is more accurate and faster. Nevertheless, it has been shown that visually determining bacterial health by observing bacterial cell morphology is a viable option if live/dead staining is not available [25, 42]. In addition, to more accurately relate the current research to real-life situations of IAIs, the used nanopattern materials could be changed. It might be important to repeat the current experiments using titanium wafers and nanopatterns instead of the silicon and platinum used in this research, as titanium is an often used material for implants and implant surfaces.

As stated before, the trend (Figure 17) shows higher bactericidal efficiencies at lower interspace distances. To be able to test bactericidal efficiencies of nanopatterns with even smaller interspace distances, the nanopillar diameters could be reduced. Although it has been determined the combination of interspace and diameter has significant influence on the bactericidal efficiency of nanopatterns [49], it is not entirely clear whether the influence of diameter is mainly due to changing the effective interspace (smaller diameters cause a larger gap between pillars), or due to the change in pillar shape (smaller diameters at the same height cause steeper pillar slopes). Because of this, care should be taken in the amount of diameter reduction that is applied. At least for 50-70 nm diameters it was observed that nanopattern are bactericidal against *S. aureus*, as found by observing dragonfly wings [51]. Of course, it is also possible to first research the effect of diameter on the bactericidal efficiencies, prior to performing the reduced interspace experiments.

5. Conclusion and outlook

As implant associated infections continue to cause devastating problems for patients, a method to prevent them would be bactericidal surfaces. To examine the bactericidal characteristics of such surfaces, nanopatterned surfaces consisting of a nanopillar grid have been produced using EBID. These nanopillars were designed to be ~180 nm in height and ~80 nm in diameter. The influence of interpillar-spacing and pillar disorder on bactericidal efficiencies of nanopatterns has been tested, which was done by producing four different nanopatterns, with interspaces of 100, 170, 300 and 500 nm. For the 170, 300 and 500 nm interspace nanopatterns a disordered version (in contrast to the true-square arranged ordered version) was produced as well, with 45, 110 and 210 nm disorder respectively. The bactericidal efficiencies for *S. aureus* of these nanopatterns were calculated based on the amount of damaged and healthy bacterial cells found on the nanopatterned surfaces. The ordered 100, 170, 300 and 500 nm interspace nanopatterns had bactericidal efficiencies of 62.3 ± 23.1%, 45.0 ± 31.4%, 8.6 ± 4.2% and 3.7 ± 2.3% respectively. The disordered 170, 300 and 500 nm interspace nanopatterns were found to have bactericidal efficiencies of 45.9 ± 29.2%, 14.7 ± 7.2% and 12.7 ± 9.8% respectively. Statistical analysis showed that lower-interspace nanopatterns performed significantly better at killing/damaging *S. aureus*, in addition to the disordered patterns performing slightly better than their respective ordered version (however non-significantly). This slight improvement of disordered over ordered nanopatterns and low-interspace over high-interspace nanopatterns could be explained by the increased local pillar densities, which are believed to cause higher amounts of stress on the bacterial cell walls. In addition, the rough surface is thought to complicate cell mobility and in turn causing cell damage, as no significant difference between bacterial densities on and around the nanopatterned areas was found. This increase in stress is thought to cause cell rupturing and subsequent cell death, although further investigations are needed to determine this exactly.

Further research will be needed with regards to the exact killing mechanisms of nanopatterns. In order to be able to investigate nanopatterns with lower interspaces than 100 nm, the influence of pillar diameter should be determined. Besides this, the accuracy of bactericidal efficiency measurements could be increased by using a method such as live/dead staining as the main assessment method. Another method to increase the measurement accuracy is by upscaling the experiments, producing nanopatterned areas of e.g. 3 × 3 mm^2. This upscaling could be achieved by using techniques such as parallel EBID and/or NIL. In addition, bactericidal efficiencies closer to real-life cases of IAI prevention can be determined by testing titanium nanopatterned surfaces, instead of silicon and platinum.

Appendix

A1. Bacterial growth curve

Using Synergy 2 microplate reader (BioTek, Winooski, VT, USA), live OD_{600} measurements were performed on three wells in a 24-well plate containing 1 mL *S. aureus* and BHI mixture of 0.1 OD_{600}, as well as one well containing 1 mL of BHI broth, as a control well. This process was performed under the same conditions at which the samples submerged in 0.1 OD_{600} *S. aureus* and BHI mixture would be incubated, which is at 37°C and 0 RPM (no shaking). Each time, each well was measured at 21 locations (Figure 22), of which the average was defined to be the measurement value. Figure 23 displays the resulting bacterial growth curves, displaying similar growth trends between the three bacterial wells.

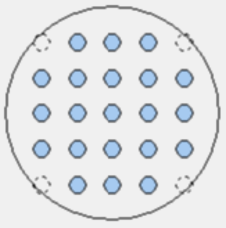

Figure 22. Using a microplate reader, each well from a 24-well plate was read at 21 different locations.

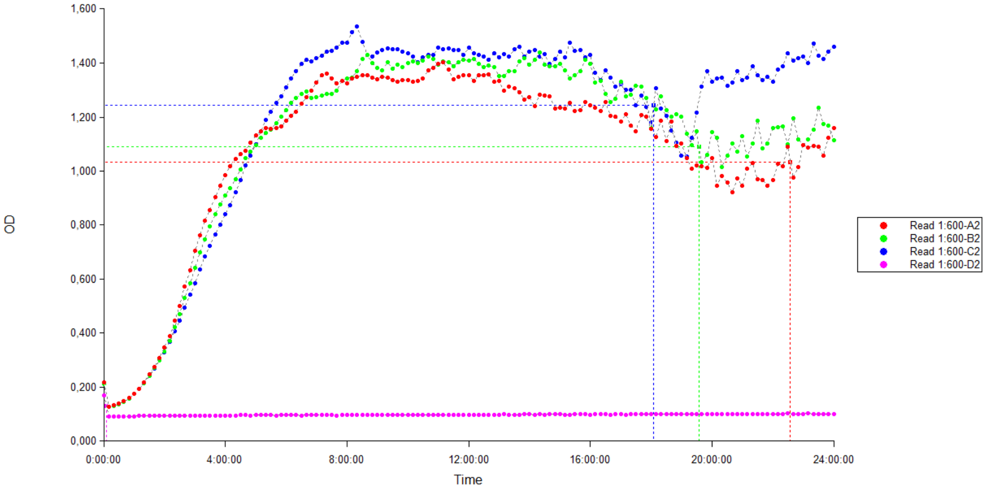

Figure 23. Bacterial growth curve of *S. aureus*. Live OD (λ=600 nm) measurements on *S. aureus* solutions (1 mL, OD_{600} = 0.1) performed every 10 minutes for 24 hours.

After about 19 hours, rapid fluctuations in the OD become apparent, which may be attributed to cell starvation due to lack of nutrients or oxygen. These dead cells may become a food source for the live cells, which causes deaths and growths in the culture. In addition, OD measurements with the used microplate reader become inaccurate once 1.0 OD is reached. To be able to use the bacteria outside of their exponential growth phase (which causes rapid bacterial proliferation) for the bacterial experiment, the incubation periods were set to 18 hours.

A2. Bacterial counting

In order to assess the amount of bacteria that are applied to the nanopatterned samples, bacterial counting was performed. To do this, six petri dishes with solid BHI agar were prepared by heating the BHI agar to liquid phase and pouring it into the petri dishes. A preculture of *S. aureus* in liquid BHI, that has been incubated in the incubator-shaker for 18 hours at 140 RPM and 37°C, was taken as the source of *S. aureus* bacteria. This preculture was diluted to 1.0 OD_{600}. Next, this dilution was diluted, in multiple steps, towards a dilution of 10^8. To do so, each time 100 µL of the previous dilution was added to 900 µL of liquid BHI, so that each step forms a 10-times diluted mixture. From the solutions that were diluted 10^6, 10^7 and 10^8 times 100 µL was drawn and applied to the solid BHI agar-containing petri dishes by smearing, to ensure formation of discrete bacterial colonies. For each of these dilutions, two petri dishes were used to gain a more accurate average amount of bacteria. These bacteria-containing petri dishes were then incubated at 37°C overnight to allow for the colonies to grow. Figure 24 shows the resulting colony-containing petri dishes, which were then used to count the amount of colony forming units (CFU) on its surface.

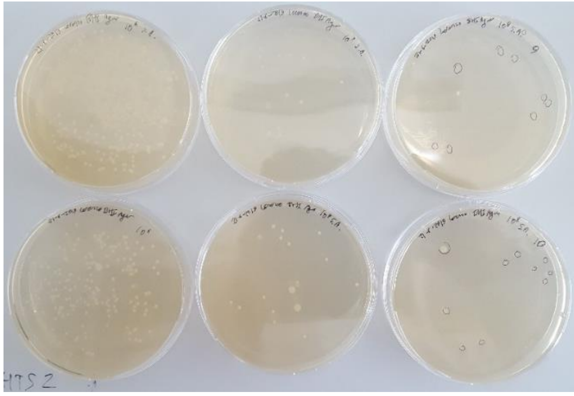

Figure 24. Colonies of *S. aureus*, formed from liquid BHI dilutions of 10^6, 10^7 and 10^8 times respectively, starting from 1.0 OD_{600}.

The counting resulted in 84 and 121 colonies on the 10^6 times diluted plate (186 and 241 for the second experiment), 6 and 14 colonies on the 10^7 times diluted plate (16 and 19 for the second experiment), and 0 and 1 colonies on the 10^8 times diluted plate (9 and 10 for the second experiment). To obtain an average value, the results from the 10^6 and 10^7 times diluted plates were added and its average was taken, which gives 147.75×10^6 CFU/100 µL from a solution of 1.0 OD_{600}. Recalculation for the amount of bacteria that is applied to the nanopatterned samples, for which a solution of 0.1 OD_{600} is used, results in a total value of 147.75×10^6 CFU/mL.

A3. Fixation times

In previous research [35], a fixation time (the duration for which the bacteria-containing samples are kept submerged in the fixation solution at 4°C) of 2 hours was used. To see if this time could be shortened, as to minimize the total time needed to perform the experiments, a few short tests were performed with regards to varying fixation times. To do so, the entire bacterial procedure was applied to flat silicon samples (without nanopatterns), with varying fixation times. The chosen fixation times were 20, 45, 60 and 120 minutes (of which the latter was used as a control sample). Following the standard procedure, these samples were then imaged using SEM to determine if the amount of bacteria in an area of 20 × 20 µm^2 (the total nanopattern area) was high enough to allow for more data to be collected per bacterial test. Figure 25 displays these SEM images.

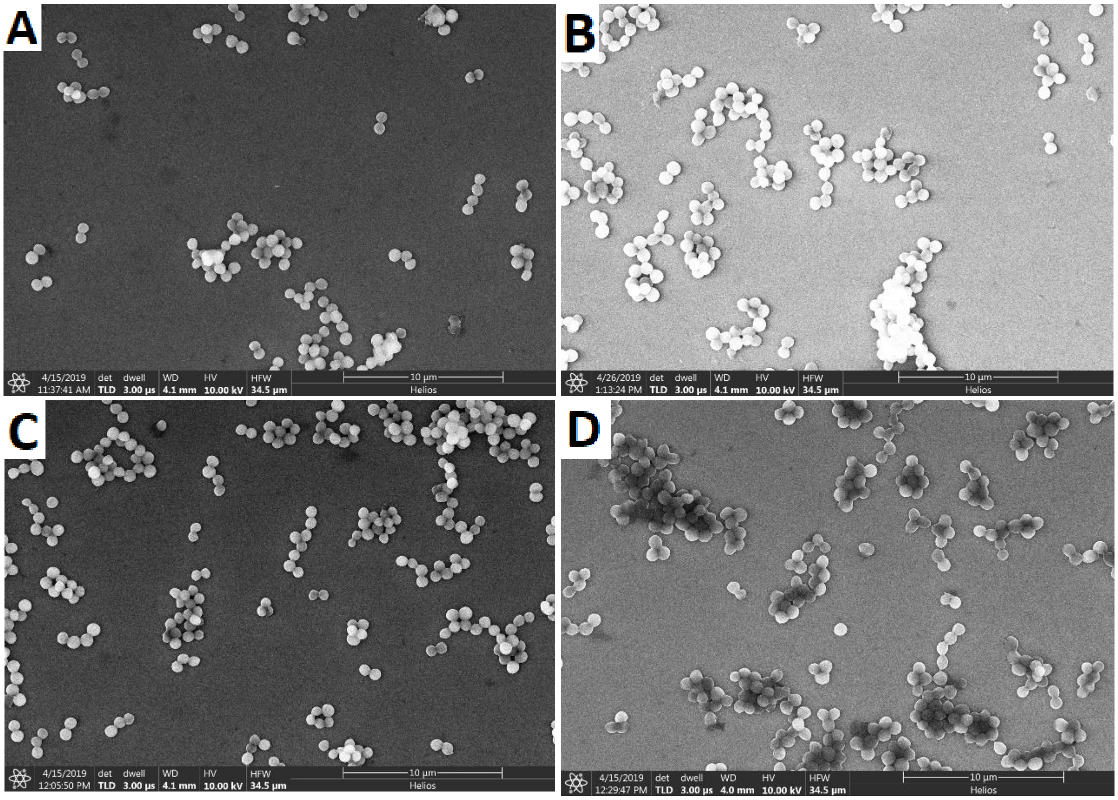

Figure 25. SEM imaging performed on flat silicon samples treated with a fixation time of **A.** 20, **B.** 45, **C.** 60 and **D.** 120 minutes to determine the bacterial density in a 20 × 20 µm^2 area. Images made at a horizontal field width of 34.5 µm.

The amount of bacteria per 20 × 20 µm^2 were 76, 102, 119 and 173 for fixation times of 20, 45, 60 and 120 minutes respectively. Bacterial distributions were not perfectly homogeneous, which resulted in some empty areas in the case of fixation times of 20 and 45 minutes. Based on these results and to ensure enough bacteria would be present on the nanopatterned areas, it was chosen to use a 60 minutes fixation time for the bacterial experiments.

A4. Healthy, deformed and dead bacterial counts

The amount of healthy, deformed and dead bacteria have been displayed in Table 4 and Table 5 for the ordered and disordered patterns, respectively. The bacterial densities of the flat (non-patterned) areas surrounding the nanopatterns have also been included, based on the amount of bacteria per 20 × 20 µm^2.

Table 4*: Assessment of bacterial cell health based on morphological observations for nanopatterns without disorder. Three patterns (20 × 20 µm^2) per sample were assessed. A tilde (~) marks a value when the number of cells was uncountable due to stacking of bacteria or other visual obstructions that inhibited counting, indicating the value was based on an estimate. The flat (non-patterned) area bacterial densities have been determined by counting bacteria in 20 × 20 µm^2 areas.*

Interspace [nm]	**Healthy cells [amount]**	**Deformed cells [amount]**	**Dead cells [amount]**	**Bactericidal efficiency [%]**	**Flat area bacterial density [amount]**	**Flat area bacterial density [amount/µm^2]**
100	4/5/10	2/1/3	5/1/8	63.6/28.6/52.4	40/46/105/40	0.10/0.12/0.26/0.10
100 (*duplicate*)	3/1/0	2/1/0	3/1/3	62.5/66.7/100	4/9/10/8	0.01/0.02/0.03/0.02
170	~111/~257/-	~34/~42/-	~18/~26/-	31.9/20.9/-	~513/471/~372/~589	1.28/1.18/0.93/1.47
170 (*duplicate*)	19/0/10	7/0/5	3/1/1	34.5/100/37.5	39/10/30/31	0.10/0.03/0.08/0.08
300	117/111/103	4/15/6	7/7/2	8.6/16.5/7.2	91/65/185/138	0.23/0.16/0.46/0.35
300 (*duplicate*)	113/149/162	8/5/1	2/6/6	8.1/6.9/4.1	~401/123/122/116	1.00/0.31/0.31/0.29
500	41/124/~164	2/9/0	0/1/2	4.7/7.5/~1.2	48/58/37/-	0.12/0.15/0.09/-
500 (*duplicate*)	351/413/219	7/5/8	0/5/2	2.0/2.4/4.4	143/272/~389/278	0.36/0.68/0.97/0.70

***Table 5**: Assessment of bacterial cell health based on morphological observations for nanopatterns with maximum disorder. Three patterns (20 × 20 µm^2) per sample were assessed. A tilde (~) marks a value when the number of cells was uncountable due to stacking of bacteria or other visual obstructions that inhibited counting, indicating the value was based on an estimate. The flat (non-patterned) area bacterial densities have been determined by counting bacteria in 20 × 20 µm^2 areas.*

Interspace [nm]	**Disorder distance [nm]**	**Healthy cells [amount]**	**Deformed cells [amount]**	**Dead cells [amount]**	**Bactericidal efficiency [%]**	**Flat area bacterial density [amount]**	**Flat area bacterial density [amount/µm^2]**
170	45	122/~319/182	23/~90/42	13/~25/22	22.8/26.5/26.0	~578/~650/~592/~618	1.45/1.63/1.48/1.55
170 (*duplicate*)	45	2/2/0	1/0/0	1/2/1	50.0/50.0/100	12/17/12/8	0.03/0.04/0.03/0.02
300	110	56/81/94	10/4/19	8/10/7	24.3/14.7/21.7	103/56/104/68	0.26/0.14/0.26/0.17
300 (*duplicate*)	110	120/107/179	3/9/6	6/7/8	7.0/13.0/7.3	266/219/207/234	0.67/0.55/0.52/0.59
500	210	70/94/37	12/13/5	8/7/7	22.2/17.5/24.5	64/83/112/143	0.16/0.21/0.28/0.36
500 (*duplicate*)	210	230/133/140	9/2/4	0/4/2	3.8/4.3/4.1	78/49/103/156	0.20/0.12/0.26/0.39

A5. Electron-beam induced deposition: Electron scattering

With regards to the EBID process, there are factors which limit EBID resolution. When the primary electrons (PE) collide with the solid substrate, they change their trajectory. These collisions may be inelastic, in which case part of the initial energy of the PE is transferred to other electrons already present in the substrate. Due to this energy transfer, low energy (< 50 eV) secondary electrons (SE) are formed. Another case is when the PEs travel through the substrate and are subsequently deflected back towards the substrate surface, forming high energy (> 50 eV) backscattered electrons (BSE) [28] (Figure 26). SEs influence accuracy by creating nonlocal effects, being largely responsible for the lateral structural growth [53]. BSEs, on the other hand, are known to cause the so-called “proximity effect”. The proximity effect occurs when pillars are close to the pillar that is being exposed to the electron beam. Due to the proximity of the pillars, BSEs are deflected towards surrounding pillars and are able to cause additional, unwanted material deposition and thus broadening of the structures [54]. In addition, the optimization of the EBID process is not only dependent on these discrepancies: focused probe optics (beam acceleration voltage, beam current, imaging performance), the substrate (material, temperature, conductivity, cleanliness) and gas delivery (precursor type, precursor temperature, pressure, molecular flux at the substrate surface) influence the morphology of the deposited structures. Additionally, as stated before, parameters that control the total exposure time of a structure (for example dwell time) directly affect the shape of the structure and should be optimized to get the exact result that is preferred.

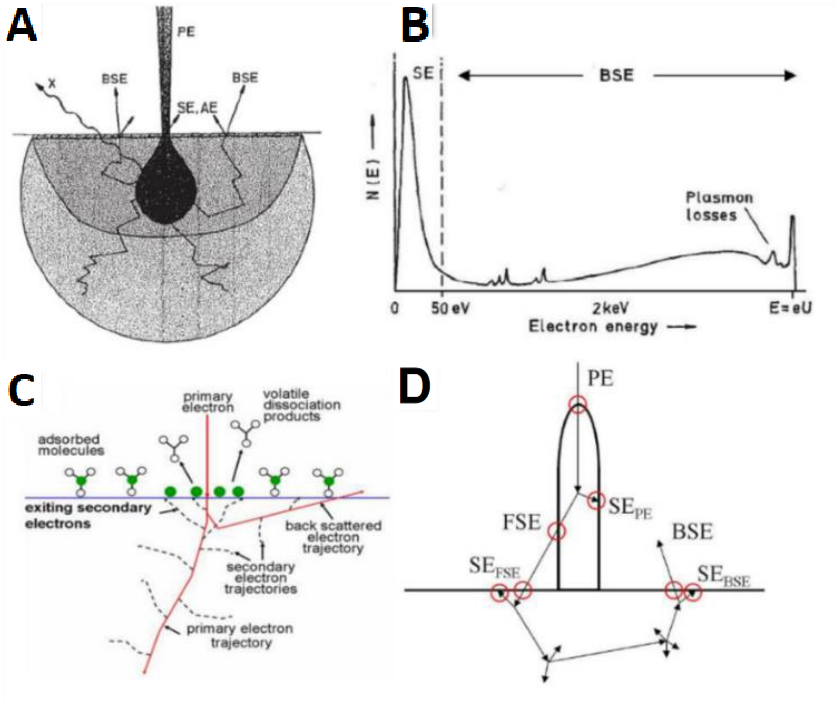

Figure 26: Schematic representations of electrons from an electron beam. **A.** Drop-shaped volume of electron scattering events for a flat substrate. **B.** A typical energy spectrum of emitted secondary electrons (SEs) and backscattered electrons (BSEs). A clear divide between the SE energy level and BSE energy level is seen at 50 eV. **C.** The trajectories electrons fired from an electron beam follow, including the SE and BSE trajectories. **D.** A deposited structure that is exposed to the electron beam. The trajectories of SEs and BSEs show how the proximity effect and other nonlocal deposition can occur due to deflection by the structure itself [54].

A6. Nanopattern fabrication: Stream files

Stream files are files that can be read by the SEM system and contains the coordinates and exposure instructions for the structure fabrication. Two example stream files are shown in Figure 27. For the right stream file an extra column is present, introducing blanking of the beam. When the beam is blanked, no electrons are fired and as such no deposition occurs, effectively adding a refresh-step to the process. The way this stream file handles refresh time is adding a refresh-step before and after each deposition step.

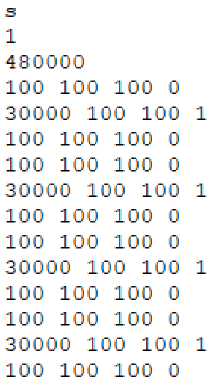

```
s
1
480000
100 100 100 0
30000 100 100 1
100 100 100 0
100 100 100 0
30000 100 100 1
100 100 100 0
100 100 100 0
30000 100 100 1
100 100 100 0
100 100 100 0
30000 100 100 1
100 100 100 0
```

Figure 27. An example stream file. This image shows a stream file with 1 pass, with 480,000 patterning steps. The patterning steps number is comprised of the *number of locations* × *repeats* × *blanking steps*. As for this stream file there are 40 pillar rows columns, 100 repeats and the beam is blanked before and after every exposure step, this results in (40 × 40) × 100 × 3 = 480,000. The other rows contain the dwell time in the first column (3 ms) and the x- and y-coordinates in the second and third columns respectively. The fourth column determines beam blanking, which is 0 to blank the beam and 1 to un-blank it.

The MATLAB script dictates the coordinates of the pillars in a pixel-based manner, meaning the interspace (defined as pillar centre-to-centre distance) has the unit [pixels]. To accurately transcribe the digital unit [pixels] into the physical unit [metres], the electron microscope horizontal field width (HFW) was set to 8.19 µm, at which magnification each pixel is equal to 2 nanometres (for example, an interspace of 170 nm is written in MATLAB as 170/2 = 85 px). As it is not possible for the electron microscopes to deposit highly accurate pillars (as accuracy is influenced by magnification) outside its field of view (its limits being 8190 × 6980 nm at a HFW of 8.19 µm, measured from the graphical user interface of the Nova software), the stream file was limited to these dimensions by limiting the amount of pillar rows and columns per array. Thus, to produce nanopatterns spanning a total area of 20 × 20 μm^2, the stream file has to be written at multiple neighbouring locations (a single written stream file being called an "array"). As each relocation of the stage results in focus loss, the relocation distance has to be reduced as much as possible. For this reason, a serpentine writing strategy was used to relocate for multiple iterations of the stream file, shown in Figure 28. Additionally, to minimize the focus lost after multiple consecutive stage shifts, the focus was readjusted after every four arrays.

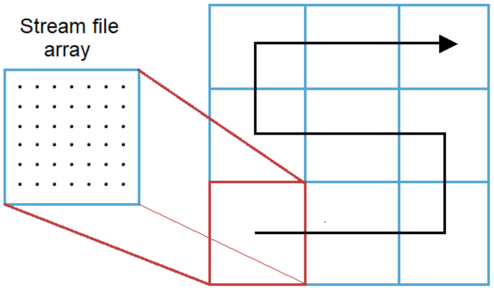

Figure 28. Serpentine writing strategy: step and repeat process to increase the total area of patterning.

A7. Nanopattern fabrication: Additional parameters

In addition to the other variables used, an extra variable was introduced with respect to the previously performed research, namely the disorder distance. This variable determines the maximum distance a pillar can be displaced (in any 360° direction) from the true-square arrangement. For this research, the disorder distance was set to the maximum distance at which pillars do not intersect when displaced towards each other, see Figure 29. As the diameter of the pillars is set to be ~80 nm, the maximum possible disorder distance can be calculated based on the following formula:

$$disorder\ distance_{max} = \frac{1}{2} * (interspace - diameter)$$

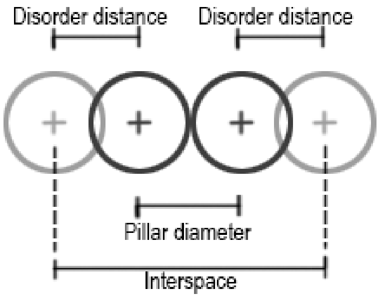

Figure 29. Pillars displaced towards each other by the random disorder angle. To avoid intersecting pillars, disorder distance should be chosen based on the interspace and diameter of the pillars.

Another new variable, one that is available in the Nova and Helios software, is blur. Blur forces a defocus upon the deposition process by shifting the focus a specified distance away from the normal focal point. This causes deposition to occur while the beam is unfocused, increasing the diameter and reducing the height of the produced pillars. This parameter is used for example in the case of the 300 and 500 nm interspace patterns. The lower amount of proximity effect that occurs due to pillars being further apart allows for more accurate deposition, which causes pillars to be higher, but smaller in diameter, with respect to the 170 nm interspace pattern designed in previous research [35]. Blur enables for these pillars to still achieve the same dimensions as those in the 170 nm interspace patterns.

A8. Nanopattern fabrication: Pattern overview

A 20 × 20 µm^2 nanopatterned area has been shown at low magnification for each of the nanopattern designs in Figure 30.

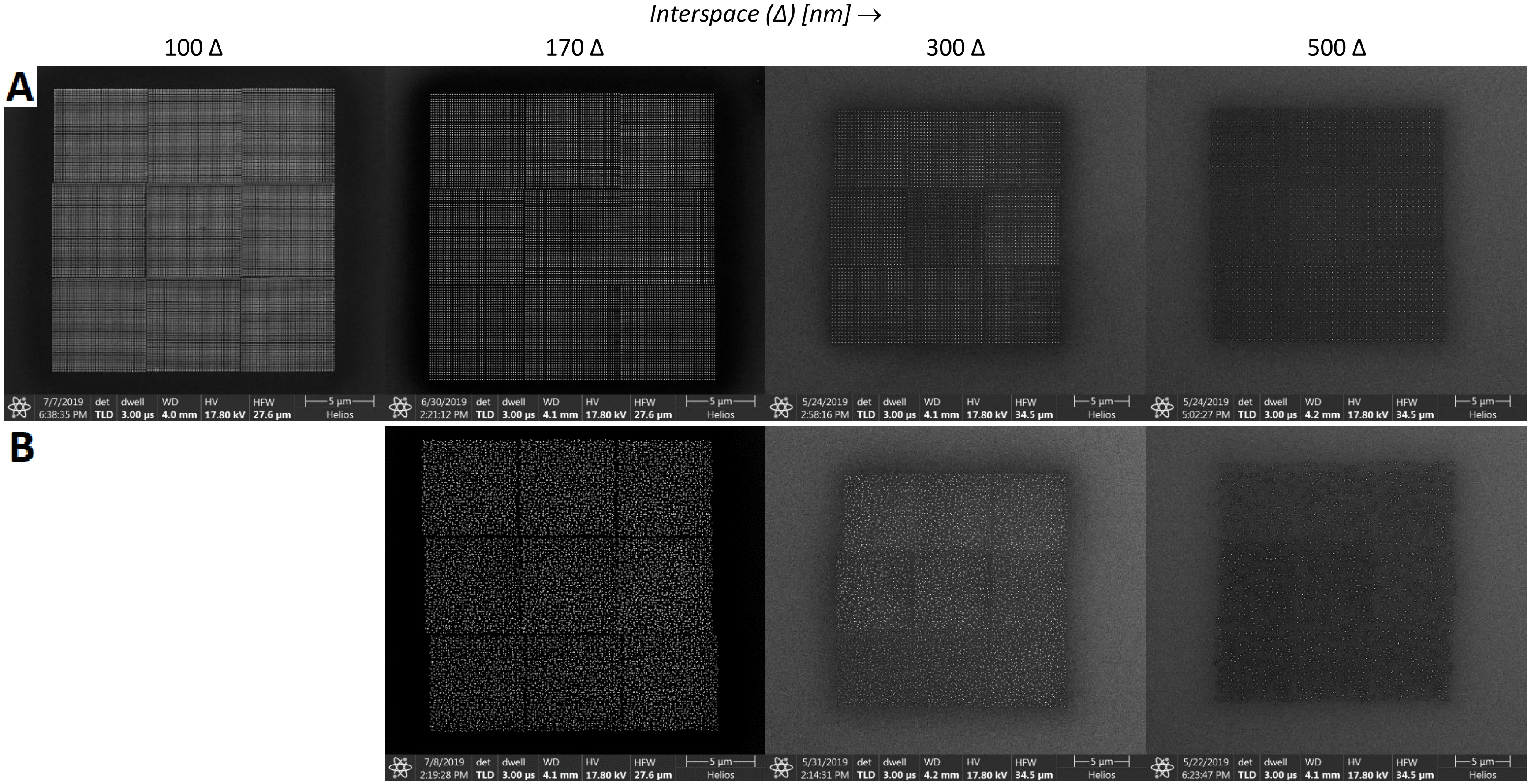

Figure 30. SEM images of the 20 × 20 µm^2 nanopatterns with different interspaces (Δ) and maximum disorder distances (Ψ) at low magnification. **A.** Overviews of the ordered nanopatterns. **B.** Overviews of the disordered nanopatterns, with Ψ = 0, 45 and 110 nm from left to right.

A9. MATLAB Script

```
%% Author: Lorenzo Kunkels
% This script forms a stream file from the defined pattern (either with or
without disorder)
% - You only have to change the "Modifiable variables" part of this script
% - In the "Modifiable variables" [DISORDER] marks variables that are only
%   used when enable_disorder is true.
% - Be sure to change the enable_disorder variable to define whether you do
%   or do not want the pattern to contain disorder.

clear all
close all
clc

% Initialize
global dwelltime;
s = create_streamfile();    % An empty streamfile is produced using the
create_streamfile function

%% Modifiable variables
% Pattern mode variable
enable_disorder = 0;              % Determines whether the pattern will
contain disorder. Set to 1 for disorder, set to 0 for no disorder.

% Beam control variables
passes = 1;                      % The number in the second row, indicating
the amount of times the streamfile is repeated
dwelltime = 60000;               % The number in the first column, in steps
of 0.1us
repeats = 50;                    % Number of times each point is dwelled
before moving on to the next point
refreshtime = [100, 100];          % [OPTIONAL] Refreshtime in steps of 0.1
us. Used if repeats are more than 1, to let the precursor gas settle (not
depleting it)

% Pattern variables ([rows] x [columns]) with [spacing] pixels inbetween (at
15625x magnification, so 1px = 2nm)
spacing = 50;                    % How far each point in the pattern is
spaced apart, in px
rows = 67;                       % Amount of rows
columns = rows;                  % Amount of columns
disorder = 0;                   % [DISORDER] Distance of random disorder, in
px

% Pillar variables ([OPTIONAL], used for calculating recommended settings and
other non-influential variables)
pillar_diameter = 40;            % Diameter of the pillars, in px
pillar_diameter_sd = 0;        % Standard deviation of the pillar diameter,
in px. Set to 0 for the ideal case in which the deposition is 100% accurate

% Extra variables ([OPTIONAL])
filename_suffix = '';               % Adds this to the filename, useful for
adding annotations
```

```
%% Square arrangement loop (create pattern)
% The starting coordinates are just where the pattern is automatically
% placed on the screen in the NovaBeam software. The screen is about
% 4095 x 3490 pixels (width x height), so the full pattern should be within
% these dimension (anything not on screen is not deposited).
% The script also makes sure no pillars are printed at negative positions
% (i.e. (x,y) = (-150, 50)), because the write_streamfile doesn't take
% signed integers, so best to avoid it altogether.

% Initial (x,y)-coordinates
xc(1) = 100;
yc(1) = 100;
if enable_disorder == 1
    xc(1) = xc(1) + disorder;
    yc(1) = yc(1) + disorder;
end

% Using the first x- and y-locations to produce a square array
for n = 2:rows
    yc(n) = yc(n-1)+spacing;
end
for n = 2:columns
    xc(n) = xc(n-1)+spacing;
end

% Create a matrix containing all locations ([x; y] matrix)
n = 1;
for xcenter = xc
    for ycenter = yc
        if enable_disorder == 1
            % Disorder streamfile
            % For every location a disorder is superimposed under a random
angle
            angle = 2*pi*rand; % Disorder angle, a random number between [0,
2pi]
            a = xcenter + disorder * cos(angle);
            b = ycenter + disorder * sin(angle);
            locations(:,n) = [int16(a); int16(b)];
        else
            % Order streamfile
            locations(:,n) = [xcenter; ycenter];
        end
        n = n + 1;
    end
end

%% Add pattern to streamfile
% Here all locations are put into the streamfile using the add_dot function
(as refresh time is used).
% With many repeats the file can become large, and it may take a while to
% write. Therefore progress is displayed while running the script.

disp('Creating streamfile ...')
for n = 1:size(locations,2)
    disp(['Location ' num2str(n) '/' num2str(size(locations,2))])
    s = add_dot( s, locations(1,n), locations(2,n), dwelltime, refreshtime,
repeats );
```

```
end
disp('Streamfile done')

%% Create streamfile
% Write files into streamfile. Filename can be adjusted to include more
parameters.

% Set filename of the streamfile
filename = ['rows' num2str(rows) 'repeat' num2str(repeats) 'pass'
num2str(passes) 'dwelltime' num2str(dwelltime*0.1/1000) 'ms' '_spacing'
num2str(spacing) '_refresh' num2str(refreshtime(1))];
if enable_disorder == 1
    % Disorder filename
    filename = [filename '_disorder' num2str(disorder)];
else
    % Order filename
    filename = [filename '_order'];
end

filename = [filename filename_suffix];

% Create the files
write_streamfile( s, [filename '_.str'], passes );
str2png( s, [filename '_.png'] )

%% Display process information and error/warning log
disp(' '), disp('========================'), disp(' ')
disp('PROCESS FINISHED')
if enable_disorder == 1
    disp('Pattern mode: Disorder')
else
    disp('Pattern mode: Order')
end
disp(' ')
disp(['File created: ' filename '_.str'])
disp('and')
disp(['File created: ' filename '_.png'])

% Display width of the pattern for the sake of reference
pattern_height_px = (rows - 1) * spacing + pillar_diameter; % Pattern height,
in px
pattern_height_um = pattern_height_px * 2 / 1000; % Pattern height, in um
pattern_distance = (pattern_height_px - pillar_diameter + spacing) * 2 *
10^(-6); % Pattern distance, in mm

disp(' ')
disp('Pattern size:')
disp([num2str(pattern_height_px) ' px || ' num2str(pattern_height_um) ' um'])
disp(['For 20x20 um, use ' num2str(ceil(20/pattern_height_um)) 'x'
num2str(ceil(20/pattern_height_um)) ' patterns. For 40x40 um, use '
num2str(ceil(40/pattern_height_um)) 'x' num2str(ceil(40/pattern_height_um)) '
patterns'])
disp([])

disp(' ')
disp(['Distance between patterns: ' num2str(pattern_distance) ' mm'])
```

References

1. Zimmerli, W., A. Trampuz, and P.E. Ochsner, *Prosthetic-joint infections.* N Engl J Med, 2004. **351**(16): p. 1645-54. Doi: 10.1056/NEJMra040181

2. Arciola, C.R., D. Campoccia, and L. Montanaro, *Implant infections: adhesion, biofilm formation and immune evasion.* Nature Reviews Microbiology, 2018. **16**(7): p. 397-409. Doi: 10.1038/s41579-018-0019-y

3. Berbari, E.F., et al., *Prosthetic joint infection due to Mycobacterium tuberculosis: a case series and review of the literature.* American journal of orthopedics (Belle Mead, N.J.), 1998. **27**(3): p. 219-227. Doi:

4. Rodriguez-Contreras, A., et al., *Antimicrobial PHAs coatings for solid and porous tantalum implants.* Colloids Surf B Biointerfaces, 2019. **182**: p. 110317. Doi: 10.1016/j.colsurfb.2019.06.047

5. Kurtz, S.M., et al., *Are We Winning or Losing the Battle With Periprosthetic Joint Infection: Trends in Periprosthetic Joint Infection and Mortality Risk for the Medicare Population.* J Arthroplasty, 2018. **33**(10): p. 3238-3245. Doi: 10.1016/j.arth.2018.05.042

6. Neoh, K.G., et al., *Balancing osteoblast functions and bacterial adhesion on functionalized titanium surfaces.* Biomaterials, 2012. **33**(10): p. 2813-22. Doi: 10.1016/j.biomaterials.2012.01.018

7. Hasan, J., R.J. Crawford, and E.P. Ivanova, *Antibacterial surfaces: the quest for a new generation of biomaterials.* Trends Biotechnol, 2013. **31**(5): p. 295-304. Doi: 10.1016/j.tibtech.2013.01.017

8. Wang, Y., et al., *Length-Scale Mediated Differential Adhesion of Mammalian Cells and Microbes.* Advanced Functional Materials, 2011. **21**(20): p. 3916-3923. Doi: 10.1002/adfm.201100659

9. Bakhshandeh, S., et al., *Simultaneous Delivery of Multiple Antibacterial Agents from Additively Manufactured Porous Biomaterials to Fully Eradicate Planktonic and Adherent Staphylococcus aureus.* ACS Appl Mater Interfaces, 2017. **9**(31): p. 25691-25699. Doi: 10.1021/acsami.7b04950

10. Hirschfeld, J., et al., *Long-term release of antibiotics by carbon nanotube-coated titanium alloy surfaces diminish biofilm formation by Staphylococcus epidermidis.* Nanomedicine, 2017. **13**(4): p. 1587-1593. Doi: 10.1016/j.nano.2017.01.002

11. Croes, M., et al., *Antibacterial and immunogenic behavior of silver coatings on additively manufactured porous titanium.* Acta Biomater, 2018. **81**: p. 315-327. Doi: 10.1016/j.actbio.2018.09.051

12. van Hengel, I.A.J., et al., *Selective laser melting porous metallic implants with immobilized silver nanoparticles kill and prevent biofilm formation by methicillin-resistant Staphylococcus aureus.* Biomaterials, 2017. **140**: p. 1-15. Doi: 10.1016/j.biomaterials.2017.02.030

13. Amin Yavari, S., et al., *Antibacterial Behavior of Additively Manufactured Porous Titanium with Nanotubular Surfaces Releasing Silver Ions.* ACS Appl Mater Interfaces, 2016. **8**(27): p. 17080-9. Doi: 10.1021/acsami.6b03152

14. Loh, X.J., *Latest Advances in Antibacterial Materials.* Journal of Molecular and Engineering Materials, 2017. **05**(01). Doi: 10.1142/s2251237317400019

15. Elbourne, A., R.J. Crawford, and E.P. Ivanova, *Nano-structured antimicrobial surfaces: From nature to synthetic analogues.* J Colloid Interface Sci, 2017. **508**: p. 603-616. Doi: 10.1016/j.jcis.2017.07.021

16. Panacek, A., et al., *Bacterial resistance to silver nanoparticles and how to overcome it.* Nat Nanotechnol, 2018. **13**(1): p. 65-71. Doi: 10.1038/s41565-017-0013-y

17. Enright, M.C., et al., *The evolutionary history of methicillin-resistant Staphylococcus aureus (MRSA).* Proc Natl Acad Sci U S A, 2002. **99**(11): p. 7687-92. Doi: 10.1073/pnas.122108599

18. Dobbenga, S., L.E. Fratila-Apachitei, and A.A. Zadpoor, *Nanopattern-induced osteogenic differentiation of stem cells – A systematic review.* Acta Biomaterialia, 2016. **46**: p. 3-14. Doi: 10.1016/j.actbio.2016.09.031

19. Dalby, M.J., N. Gadegaard, and R.O. Oreffo, *Harnessing nanotopography and integrin-matrix interactions to influence stem cell fate.* Nat Mater, 2014. **13**(6): p. 558-69. Doi: 10.1038/nmat3980

20. Ghosh, S., et al., *Analysis of killing of growing cells and dormant and germinated spores of Bacillus species by black silicon nanopillars.* Sci Rep, 2017. **7**(1): p. 17768. Doi: 10.1038/s41598-017-18125-z

21. Linklater, D.P., et al., *Comment on "Bactericidal Effects of Natural Nanotopography of Dragonfly Wing on Escherichia coli".* ACS Appl Mater Interfaces, 2017. **9**(35): p. 29387-29393. Doi: 10.1021/acsami.7b05707

22. Hasan, J., et al., *Selective bactericidal activity of nanopatterned superhydrophobic cicada Psaltoda claripennis wing surfaces.* Appl Microbiol Biotechnol, 2013. **97**(20): p. 9257-62. Doi: 10.1007/s00253-012-4628-5

23. Izquierdo-Barba, I., et al., *Nanocolumnar coatings with selective behavior towards osteoblast and Staphylococcus aureus proliferation.* Acta Biomater, 2015. **15**: p. 20-8. Doi: 10.1016/j.actbio.2014.12.023

24. Modaresifar, K., et al., *Bactericidal effects of nanopatterns: A systematic review.* Acta Biomater, 2019. **83**: p. 29-36. Doi: 10.1016/j.actbio.2018.09.059

25. Widyaratih, D.S., et al., *Towards osteogenic and bactericidal nanopatterns?* Nanotechnology, 2019. **30**(20): p. 20LT01. Doi: 10.1088/1361-6528/ab0a3a

26. Green, D.W., et al., *High Quality Bioreplication of Intricate Nanostructures from a Fragile Gecko Skin Surface with Bactericidal Properties.* Sci Rep, 2017. **7**: p. 41023. Doi: 10.1038/srep41023

27. Dickson, M.N., et al., *Nanopatterned polymer surfaces with bactericidal properties.* Biointerphases, 2015. **10**(2): p. 021010. Doi: 10.1116/1.4922157

28. van Dorp, W.F., et al., *Approaching the Resolution Limit of Nanometer-Scale Electron Beam-Induced Deposition.* Nano Letters, 2005. **5**(7): p. 1303-1307. Doi: 10.1021/nl050522i

29. Wnuk, J.D., et al., *Electron beam deposition for nanofabrication: Insights from surface science.* Surface Science, 2011. **605**(3-4): p. 257-266. Doi: 10.1016/j.susc.2010.10.035

30. Fedorov, A.G., et al., *Focused-electron-beam-induced processing (FEBIP) for emerging applications in carbon nanoelectronics.* Applied Physics A, 2014. **117**(4): p. 1659-1674. Doi: 10.1007/s00339-014-8628-4

31. Fowlkes, J.D., et al., *High-Fidelity 3D-Nanoprinting via Focused Electron Beams: Computer-Aided Design (3BID).* ACS Applied Nano Materials, 2018. **1**(3): p. 1028-1041. Doi: 10.1021/acsanm.7b00342

32. Seo, M.K., et al., *Controlled sub-nanometer tuning of photonic crystal resonator by carbonaceous nano-dots.* Opt Express, 2008. **16**(13): p. 9829-37. Doi: 10.1364/oe.16.009829

33. Barros, J., et al., *Lytic bacteriophages against multidrug-resistant Staphylococcus aureus, Enterococcus faecalis and Escherichia coli strains isolated from orthopedic implant-associated infections.* Int J Antimicrob Agents, 2019. Doi: 10.1016/j.ijantimicag.2019.06.007

34. Stinson, Z., S. Rosenfeld, and J.C. McNeil, *Infections Complicating Orthopedic Surgery and Implants*, in *Healthcare-Associated Infections in Children*. 2019. p. 133-151.

35. Ganjian, M., et al., *Nature Helps: Toward Bioinspired Bactericidal Nanopatterns.* Advanced Materials Interfaces, 2019. Doi: 10.1002/admi.201900640

36. Nowlin, K., et al., *Adhesion-dependent rupturing of Saccharomyces cerevisiae on biological antimicrobial nanostructured surfaces.* J R Soc Interface, 2015. **12**(102): p. 20140999. Doi: 10.1098/rsif.2014.0999

37. Watson, G.S., et al., *A gecko skin micro/nano structure - A low adhesion, superhydrophobic, anti-wetting, self-cleaning, biocompatible, antibacterial surface.* Acta Biomater, 2015. **21**: p. 109-22. Doi: 10.1016/j.actbio.2015.03.007

38. Bandara, C.D., et al., *Bactericidal Effects of Natural Nanotopography of Dragonfly Wing on Escherichia coli.* ACS Appl Mater Interfaces, 2017. **9**(8): p. 6746-6760. Doi: 10.1021/acsami.6b13666

39. Kelleher, S.M., et al., *Cicada Wing Surface Topography: An Investigation into the Bactericidal Properties of Nanostructural Features.* ACS Appl Mater Interfaces, 2016. **8**(24): p. 14966-74. Doi: 10.1021/acsami.5b08309

40. Truong, V.K., et al., *The susceptibility of Staphylococcus aureus CIP 65.8 and Pseudomonas aeruginosa ATCC 9721 cells to the bactericidal action of nanostructured Calopteryx haemorrhoidalis damselfly wing surfaces.* Appl Microbiol Biotechnol, 2017. **101**(11): p. 4683-4690. Doi: 10.1007/s00253-017-8205-9

41. Ivanova, E.P., et al., *Natural bactericidal surfaces: mechanical rupture of Pseudomonas aeruginosa cells by cicada wings.* Small, 2012. **8**(16): p. 2489-94. Doi: 10.1002/smll.201200528

42. Ivanova, E.P., et al., *Bactericidal activity of black silicon.* Nat Commun, 2013. **4**: p. 2838. Doi: 10.1038/ncomms3838

43. Kunkels, L.B., *Control of interspace and spatial arrangements of EBID nanopatterns for cell applications.* Internship report, TU Delft, 2019. Doi: n.a.

44. Linklater, D.P., et al., *Influence of nanoscale topology on bactericidal efficiency of black silicon surfaces.* Nanotechnology, 2017. **28**(24): p. 245301. Doi: 10.1088/1361-6528/aa700e

45. Tripathy, A., et al., *Natural and bioinspired nanostructured bactericidal surfaces.* Adv Colloid Interface Sci, 2017. **248**: p. 85-104. Doi: 10.1016/j.cis.2017.07.030

46. Wu, S., et al., *Nanostructured surface topographies have an effect on bactericidal activity.* J Nanobiotechnology, 2018. **16**(1): p. 20. Doi: 10.1186/s12951-018-0347-0

47. Ligeon, M.R.O., *Effective bactericidal nanopillars for E. coli and S. aureus.* MSc thesis, TU Delft, 2018. Doi: n.a.

48. Taubert, A., J.F. Mano, and J.C. Rodríguez-Cabello, *Biomaterials Surface Science*. 2013.

49. Mirzaali, M.J., et al., *In-silico quest for bactericidal but non-cytotoxic nanopatterns.* Nanotechnology, 2018. **29**(43): p. 43LT02. Doi: 10.1088/1361-6528/aad9bf

50. Vassallo, E., et al., *Bactericidal performance of nanostructured surfaces by fluorocarbon plasma.* Mater Sci Eng C Mater Biol Appl, 2017. **80**: p. 117-121. Doi: 10.1016/j.msec.2017.05.111

51. Wu, S., et al., *Role of the Surface Nanoscale Roughness of Stainless Steel on Bacterial Adhesion and Microcolony Formation.* ACS Omega, 2018. **3**(6): p. 6456-6464. Doi: 10.1021/acsomega.8b00769

52. Post, P.C., et al., *Parallel electron-beam-induced deposition using a multi-beam scanning electron microscope.* Journal of Vacuum Science & Technology B, Nanotechnology and Microelectronics: Materials, Processing, Measurement, and Phenomena, 2011. **29**(6). Doi: 10.1116/1.3656027

53. Silvis-Cividjian, N., et al., *The role of secondary electrons in electron-beam-induced-deposition spatial resolution.* Microelectronic Engineering, 2002. **61-62**: p. 693-699. Doi: 10.1016/s0167-9317(02)00515-4

54. van Dorp, W.F. and C.W. Hagen, *A critical literature review of focused electron beam induced deposition.* Journal of Applied Physics, 2008. **104**(8). Doi: 10.1063/1.2977587